Bachelo	rarbe	eit
---------	-------	-----

Zur Erlangung des akademischen Grades Bachelor of Science

Thema der Arbeit

Characterizing Snowdrift Events at Bayelva Station, Spitsbergen

eingereicht von: Paula Jack Zemann

Matrikelnummer: 636565

Gutachter/innen: Prof. Dr. Tobias Sauter

Prof. Dr. Julia Boike

Eingereicht am Geographischen Institut der Humboldt-Universität zu Berlin

Abgabe: 17.10.2025

Abstract

Snow distribution is an important factor that controls the ground thermal regime and influences permafrost thaw and glacier mass loss, because snow is a very effective insulator. These ground-snow dynamics are influenced on a microscale from redistribution of snow by wind, known as snowdrift, because it leads to heterogenous snow accumulation. Nevertheless, snowdrift is poorly researched so that models rely on wind speed as a proxy. I addressed this research gap with a detailed characterization of snowdrift events and their drivers. For this, I used 30-minutes averaged snow flux data from the acoustic FlowCapt4 sensor together with meteorological and snow data at Bayelva station from September 2024 to September 2025. I developed a quality assessment and defined snowdrift events. With this, I identified 73 snowdrift events in the season which have a great variety in their meteorological conditions, snow characteristics and their drivers. This demonstrates the complexity of snowdrift events in their drivers and frequency. Nevertheless, just one of these events accounts for 50% of the total snow transport during the whole season. The results emphasize that more integrated research is needed to further examine snowdrift events as well as evaluate their impact on the cryosphere.

Zusammenfassung

Schneeverteilung ist ein entscheidender Faktor, da Schnee wie ein Isolator wirkt und somit das thermische Regime des Bodens steuert, also das Auftauen von Permafrost, sowie den Masseverlust von Gletschern beeinflusst. Die Umverteilung von Schnee durch Wind, bekannt als Schneeverwehung, führt zu einer mikro-skaligen, heterogenen Akkumulation, welche die Boden-Schnee-Dynamik beeinflusst. Dennoch ist dieser Prozess kaum erforscht, sodass Modelle für Schneedrift oft nur auf der Windgeschwindigkeit basieren. Ich schließe diese Forschungslücke durch eine detaillierte Charakterisierung von Schneedriftereignissen und deren Ursachen. Dazu verwende ich über 30-Minuten gemittelte Messungen des Schneeflusses von dem akustischen FlowCapt4 Sensor, sowie meteorologische Daten und Schneedaten von der Station Bayelva von September 2024 bis September 2025. Ich habe eine Qualitätskontrolle entwickelt und Schneedriftereignisse definiert. Damit habe ich 73 Schneeverwehungsereignisse in der Saison identifiziert, die sich stark in ihren Schneeeigenschaften Antriebskräften meteorologischen Bedingungen, und unterscheiden. Dies zeigt die Komplexität von Schneeverwehungsereignissen hinsichtlich ihrer Treiber und Häufigkeit. Dennoch war nur ein einziges dieser Ereignisse für 50 % des Schneetransports während der gesamten Saison verantwortlich. Dies betont, wie wichtig es ist, Schneeverwehungsereignisse weiter zu untersuchen. Außerdem ist integrative Forschung notwendig, um ihre Auswirkungen auf die Kryosphäre zu bewerten.

Contents

1	Intro	oduc	tion	. 1
	1.1	Scie	entific importance and motivation	. 1
	1.2	Obje	ectives	. 2
	1.3	Sno	wdrift dynamics	. 2
	1.4	Stud	dy area: Bayelva station	. 3
2	Met	hodo	logy	. 4
	2.1	Data	a collection	. 4
	2.2	Data	a quality control	. 5
	2.3	Defi	ning thresholds for snowdrift events	. 7
	2.4	Mod	lelling erosion flux	. 8
	2.5	Stat	istical analysis of parameters and variability	11
	2.6	Vali	dation of snowdrift events	12
3	Res	ults .		13
	3.1	Ove	rview of data and flagging summary	13
	3.2	Mod	lel performance	16
	3.3	Cha	racterization of identified snowdrift events	18
	3.3.	1	Snow flux	18
	3.3.	2	Wind speed and direction	19
	3.3.	3	Snow characteristics	21
	3.3.	4	Air temperature	23
	3.3.	5	Precipitation	23
	3.4	Deta	ailed analysis of snowdrift events	24
	3.5	Vali	dation of snowdrift events	30
4	Disc	cussi	on	31
	4.1	Mod	lel performance	31
	4.2	Suit	ability of thresholds	33
	4.3	Cha	racterization of snowdrift events	35
	4.3.	1	Snow flux	35
	4.3.	2	Wind speed and direction	36
	4.3.	3	Snow characteristics	37
	4.3.	4	Air temperature	37

	4.3.	5 Precipitation	37		
	4.4	Single snowdrift events	38		
	4.5	Validation of Snowdrift Events	39		
	4.6	Limitations	40		
5	Con	nclusion	41		
6	Lite	rature	42		
7	App	endix	51		
	7.1	Dataset overview	51		
	7.2	.2 Use of AI			
	7.3	Declaration of originality	54		

List of Figures

Figure 1: Quality control flags for FC4 sensor
Figure 2: Time series of flags for FC4
Figure 3: Data overview Sept 24 - Sept 25
Figure 4: Calibration of erosion efficiency e_salt
Figure 5: Model performance using mean wind speed17
Figure 6: Model performance using max wind sped17
Figure 7: Relationship between distribution and flux of identified events, grouped by TST
Figure 8: Comparison of environmental conditions during events vs non-events 20
Figure 9: Wind direction21
Figure 10: Relationship between maximum wind speed and mean snow flux, grouped by density
Figure 11: Snowpack state and mass balance23
Figure 12: Relationship between air temperature and mean wind speed, grouped by mean snow flux
Figure 13: Snowdrift occurence after precipitation event
Figure 14: Snowdrift event 1
Figure 15: Snowdrift event 3427
Figure 16: Snowdrift event 52
Figure 17: Snowdrift event 7329
Figure 18: Sastrugi detection from snow depth dynamics
Figure 19: Temporal variability of dynamic wind speed threshold
Figure 20: Cumulative TST contribution per snowdrift event
Figure 21: Monthly TST compared with number of identified events, grouped by intensity

List of Tables

Table 1: Description of quality control flags	5
Table 2: Notation of variables and parameters	10
Table 3: Statistics of identified snowdrift events	18
Table 4: Visual validation of snowdrift events	30
Table 5: Overview of used datasets, sensors and parameters with accuracy	51

List of Abbreviations

Abbreviation	Description
Al	Artificial Intelligence
AWI	Alfred-Wegener-Institute
DSN	Snow depth
FC4	FlowCapt™ FC4 sensor by ISAW company
IQR	Interquartile range
MAE	Mean absolute error
Meteo	Meteorological
NA	Not available/ missing value (for analysis with R)
RMSE	Root mean squared error
SPARC	Sensitivity of Permafrost in the Arctic
SWE	Snow water equivalence
TST	Total snow transported
WP	Lambrecht weighing precipitation gauge rain[e]H3

Acknowledgments

I would like to thank my supervisors Prof. Dr. Tobias Sauter and Prof. Dr. Julia Boike for their support and guidance throughout my writing process, especially for taking time to discuss my work.

I also thank Prof. Dr. Julia Boike and Dr. Inge Grünberg for their constructive feedback and helpful suggestions, which helped me to improve my thesis.

Finally, I would like to thank William Cable, Niko Bornemann and Dr. Frederieke Miesner for kindly providing the data for my analysis and answering questions throughout the research process.

1 Introduction

1.1 Scientific importance and motivation

The Arctic region is widely discussed in climate debate. Even if many definitions for the Arctic exist, I limit the Arctic region geographically to the Arctic circle, so all land and water areas above the parallel 66° 33' 44" North (Federov et al., 2019; Arctic Portal, 2025). Within the Arctic, the temperature rise has more than doubled compared to the global average over the last decades, this is known as Arctic amplification (Notz and Stroeve, 2016; Richter-Menge et al., 2017; Serreze & Barry, 2011). Also, more heat and moisture are transported northwards, while less heat is lost to space from the Arctic relative to the subtropics. In a positive feedback loop, the Arctic loses ice due to the warming, which exposes the darker ocean and land areas underneath. They lead to a reduced summer albedo, which amplifies the warming (Serreze & Barry, 2011; Pithan & Mauritsen, 2014; Goosse et al. 2018; Stuecker et al., 2018). The Arctic amplification is already across the cryosphere (Meredith et al., 2019; Saigger et al., 2024). Projections show that nearsurface permafrost will decrease between 2-66%, compared to the current state, under low emission scenario RCP2.6 by the end of the century (Meredith et al., 2019; McGuire et al., 2018). Similarly, Arctic glaciers lose 212 Gigatons mass per year, which contributes to sea level rise (Meredith et al., 2019). A moderate emission scenario (RCP4.5) estimates a sea-level rise of 104 ± 17 mm by 2100 just from Arctic glaciers (Radic et al., 2013).

Furthermore, the Arctic snow cover decreases around 3-5 days per decade, even if the Arctic has the most persistent snow cover in winter, with around 8-10 months per year. This is mostly due to a later onset of snow as well as around 20% earlier spring melt per decade (Bokhorst et al., 2016; Meredith et al., 2019; Callaghan et al., 2011). Seasonal snow cover is important for the radiation balance as it has a high surface albedo. Furthermore, snow controls the ground's thermal regime as it has low thermal conductivity (e.g., Luetschg et al., 2004, 2008; Ishikawa, 2003; Goodrich, 1982; Harris et al., 2009). Snow heights from 60 to 80 centimeters effectively insulate the ground from the atmosphere (Haeberli, 1973). Additionally, snow delays permafrost and glacier thawing and influence the freshwater budget (Harris et al., 2009; Meredith et al., 2019). A redistribution of snow by wind results in spatially different ground temperatures, while the snow keeps the ground comparably warm in winter (Gruber et al., 2004; Gisnas et al., 2014). The extent of the spatial variability depends on the topography, wind speed and snow properties of the site (Gisnas et al., 2014; Isaksen et al., 2011; Etzelmüller, 2013).

According to multiple studies, the redistribution of snow is a key process to understand the local heterogenities of snow accumulation (Saigger et al., 2024; Pomeroy & Male, 1991; Callaghan et al., 2011). Nevertheless, Arctic snowdrift processes are poorly investigated and single events are overlooked due to technical limitations and scarce data availability. Models often rely on a proxy of windspeed for snowdrift (Voordendag et

1 Introduction

al., 2024; Zhang et al., 2022; Saigger et al., 2024; Pomeroy et al., 1997). I address this research gap and characterize snowdrift events using direct and high temporal resolution data of snowdrift measurements from the new installed FlowCapt4 sensor.

1.2 Objectives

Objective 1: Identify snowdrift events at Bayelva station with quality-controlled data.

To analyze snowdrift events, I first need to develop a quality assessment to exclude false values from the dataset. Furthermore, I will test thresholds to determine important events for my further analysis.

Objective 2: Model the erosion flux to predict snow erosion.

To get a better understanding of the drivers and frequency of snowdrift events, I want to model the erosion flux to predict snow erosion. I validate my model with the measured erosion derived from snow depth change on site.

Objective 3: Examine temporal variability of snowdrift as well as characterize and compare different snowdrift events.

The main goal of the thesis is the characterization of snowdrift events at Bayelva Station, Spitsbergen. I will analyze the FlowCapt4 snow mass flux together with meteorological and snow state parameters, for example wind speed, temperature, precipitation, snow depth and snow-water-equivalent (SWE). The temporal availability of the snow flux data is from September 2024 to September 2025.

Objective 4: Validate Snowdrift events.

I validate my identified snowdrift events with pictures of two ground-based webcams at the study site. Both have a frequency of approximately one picture per hour.

1.3 Snowdrift dynamics

The snow transport by wind is known as blowing and drifting snow. These two types are differentiated by height, although the exact definition varies in literature (Cogley et al., 2011; Zhang et al., 2022). Drifting snow is limited up to 2 or 2.4 meters above ground level and blowing snow begins above this. The characteristic height is chosen, because blowing snow severely restricts horizontal visibility at a certain height, while drifting snow does not reduce visibility at eye level (Cogley et al., 2011; Zhang et al., 2022).

Snow transport happens in two modes: saltation and suspension. During saltation, particles bounce and hop very close to the ground, up to 0.1 meters. Suspension starts on top of that and can go up several meters, as turbulent wind gusts lift up particles that can remain in the air over several hours (Pomeroy & Male, 1991; Gordon et al., 2009). I

analyze snowdrift in the suspension layer as the snow flux is measured much above 0.1 meters. The particle concentration in the suspension layer decreases exponentially with increasing height (Naaim et al., 1998). A particle is defined as the smallest visible unit that is part of the snowpack (Kinar, 2013; Colbeck, 1986).

The initiation of snowdrift depends on wind speed, air temperature and deposition time. Temperature and deposition time determine the particle cohesion, so the resisting force for transportation. The wind must exceed a critical threshold to overcome this cohesion, while the erosion of fresh snow is easier than older snow or larger particles that need a higher wind speed (Fabricus et al., 2025).

1.4 Study area: Bayelva station

Bayelva station is a long-term observatory in the European high Arctic on western Spitsbergen. It is located three kilometers away from the northernmost settlement of Spitsbergen: Ny-Ålesund. Due to the remote location, Bayelva station is largely unaffected by human activity (Boike et al., 2018). It is on top of the Leirhaugen hill, 25 meters above sea level, between the two mountains Zeppelinfjellet and Scheteligfjellet (Grünberg et al., 2024; López-Moreno et al., 2016). In unglaciated areas the depth of continuous permafrost is around 100 meters, with an active layer thickness from 1 to 2 meters at the end of summer (Boike et al., 2018).

Especially during winter, Bayelva is exposed to more cloudiness, precipitation and cyclones (López-Moreno et al., 2016). More clouds increase the incoming longwave radiation at the surface, which leads to higher temperatures (López-Moreno et al., 2016). The area receives around 400mm of precipitation, mostly as snow from September to May (López-Moreno et al., 2016; Boike et al., 2018). Projections also show an increase in precipitation of 5-20% annually in southwest Spitsbergen up to the end of the century (López-Moreno et al., 2016). This precipitation is highest in fall, directly followed by winter with an increase of 0.31 mm per decade. Nevertheless, this precipitation trend is entirely driven by liquid precipitation with an increase of 0.36 mm per decade, whereas snowfall shows no trend in Ny-Ålesund. However, snowfall is often underestimated by around 50% in the study, especially in stormy winters (Athulya et al., 2023).

The temperature 2024 in Ny-Ålesund in 2m height ranges from -24.4 to 5.7 °C in January with a mean of -9.9 °C and in July from 2.4 °C to 17.8 °C with a mean of 8.6 °C (Maturilli, 2020 et seq.). The change in radiation budget and atmospheric circulation patterns result in air temperature rise which affects the snowpack (López-Moreno et al., 2016).

3 Introduction

2 Methodology

2.1 Data collection

To analyze snowdrift transport, I used flux data collected by the FlowCapt (FC4) sensor as well as meteorological and snow data. All data were collected by the SPARC research group, which is dedicated to studying the Sensitivity of Permafrost in the Arctic and is part of AWI. The dataset contained three different measurement stations from Bayelva (Ba): the meteorological station BaMet2009, the characteristics of the snow at the station BaSnow2019 and the blowing snow sensor at the station BaSnow2024. My analysis time span contains one full year, starting at the setup of the FC4 sensor on September 09, 2024, till the end of my analysis on September 18, 2025.

From the meteorological dataset BaMet2009 I used the wind speed, temperature and relative humidity at a height of two meters, as well as air pressure, snow depth and precipitation. Precipitation is measured from two different sensors: a tipping bucket rain gauge that measures only liquid precipitation and a weighing precipitation gauge (WP) that measures liquid and solid precipitation. The dataset has a temporal resolution of 30-minutes summed data for precipitation and 30-minutes averaged data for the other parameters which matches the resolution of the snow flux data.

Within the snow station dataset BaSnow2009, the snow water equivalent is calculated from the measured radiation of Potassium-40 (⁴⁰K) that is naturally emitted from the soil. The more snow is on the ground, the less radiation is detected (Jentzsch et al., 2020). I also used another snow depth sensor, which is identical to the meteorological station but located directly next to the snowdrift sensor. Since the snow water equivalent data is over six-hours averaged and the snow depth 1-hour averaged, I used a forward-fill method to match the data to a 30-minutes resolution.

The BaSnow2024 dataset contains the FC4 device that measures horizontal particle flux and is the main part of my analysis. The sensor is typically used in meteorology and applied scientific research in cold regions (ISAW, 2020a). It measures only drifting snow due to the low measuring height from 0.92 meters to 1.84 meters above the ground. This mostly comprises the smaller and lighter snow particles that can travel long distances. The FC4 is an acoustic sensor. The measuring surface is a cylindrical tube with a diameter of 32 millimeters and a height of 92 centimeters (ISAW, 2020b). Inside the tube are microphones that record change in internal acoustic pressure induced from the impact of snow particles. The signal is then transmitted to a frequency analyzer and divided into particles using a Fourier transformation. As the impact of snow particles has a higher frequency, the sensor can filter out wind eddies internal (ISAW, 2020b; Jaedicke, 2001; Chritin et al., 1999). The output is proportional to particle flux Q in g m $^{-2}$ s $^{-1}$ (Chritin et al., 1999). In a frequency of 30 minutes, the output is saved with a minimum, maximum, mean and standard deviation in g m $^{-2}$ s $^{-1}$ as well as the cumulative flux in g m $^{-2}$ (ISAW, 2020a). The accuracy is \pm 5% compared to sensors of the same model (ISAW, 2020b). The

sensor also calculates the wind speed based on pressure changes within the tube, with an accuracy of \pm 15% in laminar conditions and without external parasitic turbulences or low-frequency noise (ISAW, 2020b; Doorschot et al., 2004). Nevertheless, I used the meteorological wind speed as this has a better accuracy of \pm 0.3 m s⁻¹ (R.M. Young Company, 2000).

All data are carefully quality controlled by SPARC except for the weighing precipitation gauge and the BaSnow2024 dataset. For this data, I developed a script to flag invalid values to assure data quality. All sensors' names and their accuracy as well as additional information are available in the Appendix (Table 5).

2.2 Data quality control

To flag data from the weighing precipitation gauge (WP) and FlowCapt sensor (FC4), I developed a flagging routine based on SPARC's quality control categories (Table 1). I applied clear thresholds for categories 1-4 directly. For categories 5-8, I developed a flagging routine and adjusted my flags to avoid excluding too much data that seemed plausible. Furthermore, I flagged all values in a contextually related group if one value was flagged (e.g. minimum, maximum, mean, standard deviation and cumulated sum of the parameter), because the other values may had the same error or the statistical metrics included the faulty value. Additionally, I compared the FC4 measured wind speed with the meteorological wind sensor by summing both accuracies for a wider range. If this range is exceeded, I flag the value as decreased accuracy. Finally, if multiple flags apply to a value, I assigned the lowest of these flags from 1-8 and excluded the data for further analysis. I only kept good data (flag 0) that I assigned if no other flag applied.

Table 1: Description of quality control flags (Boike et al., 2018) and my flagging routine that I developed with information from the manufacturers (Lambrecht meteo GmbH, 2025; ISAW, 2020a; ISAW, 2020b).

Flag	Meaning	Description	Implemented flagging routine
0	Good data	All quality tests passed	
1	No data	Missing value	
2	System error	Corrupted data due to system failure (e.g. power loss, sensor damage)	No information in data
3	Maintenance	Data affected by maintenance (e.g. installation, cleaning, calibration)	FC4: first six hours after setup

Flag	Meaning	Description	Implemented flagging routine
4	Physical limits	Values outside possible range or manufacturers specifications	 WP: operating temperature from -40 to +70°C; measuring range up to 600 mm per 30min FC4: operating temperature from -40 to +80 °C; maximum wind speed up to 250 km h⁻¹
5	Gradient	Unlikely spikes or prolonged constant periods	
6	Plausibility	Values unlikely in comparison with other parameters	• FC4: snowdrift without wind (maximal wind speed = 0 m s ⁻¹); snowdrift in warm conditions with air temperature > 5 °C; rain events (rain events are defined in section 2.3.1)
7	Decreased accuracy	Values differ from reference (e.g. freezing soil has no temperature of 0 °C)	 FC4: wind speed is compared with meteorological sensor while both accuracies summed (±15% for FC4 and ± 0.3 m s⁻¹ for meteorological wind speed)
8	Snow covered	Sensor is snow covered	 Snow depth is greater than sensor height

I also want to mention the flags that I excluded. I rejected a gradient test where the mean value remains constant over at least three consecutive measurement periods (\geq 1.5 hours) as this identified over 18% of data that seemed plausible. This occurs because the mean snow flux is often very small at 0.001 g m⁻² s⁻¹ and can remain constant for hours. Also, I did not account for system error (flag 2), because the required error codes were available in the data (ISAW, 2020a).

Furthermore, I manually reviewed snow flux values above the manufacturers limit of 250 g m $^{-2}$ s $^{-1}$, because the FC4 can theoretically measure the snow flux up to 1875 g m $^{-2}$ s $^{-1}$ as it transmits the signal up to 2500mV (ISAW, 2020a; Cierco et al., 2007). I decided to keep four out of five values that exceeded this limit, because they seemed plausible based on meteorological data and webcam pictures. I just rejected one value in May as I couldn't recognize any snowdrift in the webcam and the temperature was relatively high with over 1°C.

2.3 Defining thresholds for snowdrift events

To define snowdrift events, I filtered out rain which was measured by the acoustic FC4 sensor. The temperature for the transition zone from snow to rain is debated in literature with values between 0 to 2°C, whereas I used a threshold of 0.6°C which was optimized for Svalbard (Jennings et al., 2018; van Pelt et al., 2019). Additionally, I used the tipping bucket for liquid precipitation, as other authors suggest to use different methods than just a temperature threshold (Dou et al., 2021; Dutra et al., 2011). I did not use the tipping bucket alone to determine rain events as it also can measure melting snow inside the bucket (Upton & Rahimi, 2003). Even if other authors excluded snowfall events, because they lead to an underestimation in the snow mass flux, I included them as this calibration was improved in newer devices like the FC4 (Trouvilliez et al., 2015; Zhang et al., 2022). Nevertheless, I must consider snowfall in the analysis, as it provides easy erodible particles that can intensify the snow mass flux measured by the sensor (Amory, 2020).

Furthermore, snowdrift needs available snow, therefore I set the minimum snow depth to 5 centimeters to exclude disturbances i.e. caused by insects. I did not define a threshold for snow age so the duration since the last snowfall event, as I analyze this in results. Also, very high wind speeds can erode older, dense snow (Sturm et al., 2001; Trouvilliez et al., 2015).

I used a wind speed threshold to further exclude signals from insects or vibrations as no snowdrift can occur without wind. While some authors used a threshold of 6 m s $^{-1}$, I decided to use a dynamic wind speed threshold which I calculated with the friction velocity, the logarithmic wind profile and the snow density in the erosion model (chapter 2.3.2) (Pomeroy & Gray, 1995; Sturm et al., 2001). My specific wind speed threshold is based on the data from the study site and the height of the sensor.

At least three hours of high wind speeds are required to initiate an important snowdrift, therefore I used this threshold as minimum event duration, even if snowdrift can occur in a smaller period of time (Sturm et al., 2001).

In summary, a snowdrift event is defined by these criteria:

- 1. air temperature in 2 meters height is less than or equal to 0.6 °C and no liquid precipitation is measured from the tipping bucket to exclude rain events,
- 2. wind speed must pass dynamic threshold,
- 3. event must last at least 3 consecutive hours and
- 4. maximum snow flux must be at least 0.001 g m⁻² s⁻¹.

Furthermore, I will determine the importance of events by their total amount of transported snow (TST), as this is ultimately decisive for the isolation of glaciers or permafrost. The TST is calculated by summing the snow transport over all measurement periods during the event (i). For each interval, the event duration (t) is multiplied with the average snow flux and the sensors length (L) (Zhang et al., 2022).

7

$$TST\left[\frac{kg}{m}\right] = \sum_{i=1}^{1} t\left[s\right] * L\left[m\right] * MeanFlux\left[\frac{kg}{m^2 * s}\right]$$
 (1)

2.4 Modelling erosion flux

I implemented a simplified erosion model to predict snow erosion with on-site measurements using equations from Sauter et al., 2013. The model is originally built to quantify snowdrift and sublimation for blowing snow as well as drifting snow (Sauter et al., 2013). The model should provide a better understanding of the drivers of erosion which then lead to snowdrift.

The model is based on the proportionality of the erosion flux (q_e) to the excess surface shear stress (u_*^2) (Sauter et al., 2013; Anderson & Haff, 1991). All parameters with units are listed in Table 2.

$$q_e = e_{salt} * (\rho_a * u_*^2 - \rho_a * u_{th}^2)$$
 (2)

To use this dependency of the erosion flux, I substituted all unknown variables with parameters that where measured at site. I started with the threshold of the friction velocity (u_{th}) that is assumed to be proportional to the snow density (ρ_s) , because it represents the characteristics of the snowpack (Walter et al., 2004; Sauter et al., 2013).

$$u_{th} = 0.0195 + (0.021 * \sqrt{\rho_s}) \tag{3}$$

I calculated the snow density ρ_s from SWE, water density (ρ_w) and the measured snow depth (h_s) from the snow2019 station (Sturm et al., 2010). Furthermore, I decided to restrict the snow density, because it may be overestimated due to incorrect values from SWE or snow depth. For example, the SWE equivalent dramatically increases during rain events which can lead to a calculated snow density that exceeds the physical limits (e.g. > 1000 kg m⁻³). Furthermore, ice can develop during melting-freezing cycles which cause a very high density of the whole snowpack that doesn't represent the fresh, erodible snow on the surface. Therefore, I chose a conservative threshold for snow density of 600 kg m⁻³ based on my data and according to Sturm et al., 2010 and replaced higher values with NA.

$$\rho_{s} = \frac{(SWE * \rho_{w})}{h_{s}} \tag{4}$$

Moreover, I calculated the friction velocity (u_*) as it is not measured directly, therefore I use the logarithmic wind profile which describes how wind speed increases logarithmically with increasing height above the ground, as there is less friction velocity. The logarithmic wind profile puts the friction velocity (u_*) in a relationship with the mean wind speed (\overline{U}) , which was measured directly in a height of 2 meters (z). The von Kármán constant k is a universal constant and acts as a constant of proportionality (1/k) in this

case. The factor z_0 represents the aerodynamic roughness length (Stull, 1988; von Kármán, 1930).

$$\frac{\overline{U}}{u_*} = \frac{1}{k} * \ln\left(\frac{z}{z_0}\right) \tag{5}$$

Additionally, I replaced the air density ρ_a in Formula 2 with parameters that are measured at the station: temperature, relative humidity and air pressure by using the law of ideal gases (Stull, 1998). As the input pressure p is measured in hectopascals (hPa), I multiplied it by factor 100 to convert it to pascals (Pa), since 1 hPa is equal to 100 Pa. To have consistent units, I also converted the measured temperature T from Celcius to Kelvin with the operation T [K] = T [°C] + 273.15. To further calculate the air density, I changed the amount of substance n with the molar mass M with $\rho_a = \frac{m}{v}$.

$$(p * 100) * V = n * R * (T [°C] + 273.15)$$
 with $n = \frac{m}{M}$ (6)

The universal gas constant R applies to any ideal gas, but it is defined per mole. To calculate the air density, I used $R_{specific}$ to adapt for the specific gas which depends on the mass (Stull, 1998).

$$\rho_a = \frac{(p*100)}{R_{specific}*(T+273.15)}$$
 with $R_{specific} = \frac{R}{M}$ (7)

Furthermore, air is a mix of dry air and water vapor, while moist air is less dense than dry air. Especially during snowdrift events, the humidity is extremely high and is increasing as snow sublimates due to high wind speeds and energy. Therefore, I used the virtual temperature, which represents the temperature that dry air would need to have the same density of moist air at the same pressure (Formula 8). I calculated the virtual temperature with the actual temperature (T) and the specific humidity (SH) (Formula 9). The constant 0.61 accounts for the lower molecule weight of water vapor compared to dry air (Stull, 1988).

$$\rho_a = \frac{(p*100)}{R_{specific,dry}*T_v} \tag{8}$$

$$T_{\nu}[K] = (T \circ C) + 273.15 * (1 + 0.61 * SH)$$
 (9)

The specific humidity depends on the actual vapor pressure e_a . I calculated the actual water pressure with the saturation vapor pressure e_s and the relative humidity RH. This is a variation of the Magnus-Tetens equation that can be used for a plane surface of ice which is given, because the surface has a snow-ice crystal structure. The value 6.1121 (Formula 12) is a constant for the saturation water vapor [hPa] over a plane ice surface (Alduchov & Eskridge, 1996).

$$SH = \frac{0.622 * e_a}{(p - 0.378 * e_a)} \tag{10}$$

$$e_a = e_s * \frac{RH}{100} \tag{11}$$

$$e_s = 6.1121 * e^{\frac{22.587*T}{(T+273.86)}}$$
 (12)

Finally, I determined all parameters with on-site measurements, so the last step was to calibrate the model with the erosion efficiency e_{salt} (Formula 2). The erosion efficiency e_{salt} is a dimensionless, empirical parameter that quantifies how effective wind shear stress erodes snow particles. A lot of energy is converted to heat from friction or due to creating small air eddies instead of snow particle erosion. Even though the range from e_{salt} is between 0 and 1, a typical value for snow erosion is around 0.0005 (Naaim et al., 1998; Yang et al., 2022; Sauter et al., 2013). For the calibration I used the measured erosion flux that I derived from snow depth (DSN) change as a reference. Furthermore, I also validated the model by comparing the modeled erosion with the measured erosion derived from negative snow depth change.

To create this reference, I calculated the snow depth change for both stations by subtracting the snow depth of the previous time step from the current one over all periods. I defined negative snow depth changes as erosion and positive changes as accumulation. For the model calibration (formula 13), I only used the snow2019 station as this is located closer to the sensor. For further analysis of individual events, I also calculated the net snow depth change between start and end time of each event, as well as the maximum snow depth change during the event.

$$MAE = \frac{1}{n} \sum_{i=1}^{n} |modeled\ erosion - observed\ erosion\ from\ DSN\ change| \tag{13}$$

I selected the optimal e_{salt} value by minimizing the mean absolute error (MAE). I choose this error metric for the calibration as it is robust to outliers and widely used in scientific modeling approaches (Hodson, 2022). Even if other authors tend to use the root mean squared error (RMSE), because RMSE is better for normally distributed errors, it is very sensitive to outliers (Essery et al., 2013; Hodson, 2022). I calculated MAE over every 30-minutes interval, averaged this and used the e_{salt} for the lowest error.

Table 2: Notation of variables and parameters.

Notation	Parameter		Reference
e_a	actual vapor pressure [hPa]		
$e_{\scriptscriptstyle S}$	saturation vapor pressure [hPa]		Alduchov & Eskridge, 1996
e_{salt}	erosion efficiency, [0 $e_{salt} \le 1$], e_{salt} used = 0.0005	≤	Naaim et al., 1998; Sauter et al., 2013
h_s	snow depth [m]		

Notation	Parameter	Reference
k	von Kármán constant, k = 0.4	Stull, 1988
M	molar mass [kg mol ⁻¹]	
m	mass [kg]	
n	amount of substance [mol]	
q_e	erosion flux [kg m ⁻² s ⁻¹]	Sauter et al., 2013
R	universal gas constant, R \approx 8.314 [J mol ⁻¹ K ⁻¹]	Stull, 1988
$R_{specific}$	specific gas constant [J kg-1 K-1]	
$R_{specific,dry}$	specific gas constant for dry air, $R_{specific,dry} \approx 287.058 [\text{J kg}^{-1} \text{K}^{-1}]$	
RH	relative humidity [%]	
SH	specific humidity [kg kg ⁻¹]	
SWE	Snow water equivalent [m]	
T	temperature [°C]	
T_v	virtual temperature [K]	
\overline{U}	mean wind speed [m s ⁻¹]	Stull, 1988; Trouvilliez et al., 2015
u_*	friction velocity [m s ⁻¹]	Stull, 1988
u_*^2	surface shear stress [F A ⁻¹]	
u_{th}	friction velocity threshold [m s ⁻¹]	Sauter et al., 2013
V	volume [m³]	
Z	height of wind speed measurement [m]	Trouvilliez et al., 2015
z_0	aerodynamic roughness length, $z_0 \approx 0.001 [\text{m}]$	Stull, 1988
$ ho_a$	air density [kg m ⁻³]	Sauter et al., 2013
$ ho_{\scriptscriptstyle \mathcal{S}}$	fresh snow density, $\rho_{\rm S}$ = 200 [kg m $^{-3}$]	Benn & Evans, 2010
$ ho_w$	water density, $\rho_w \approx 1000 [\text{kg m}^{-3}]$	

2.5 Statistical analysis of parameters and variability

There are many factors that influence the probability of snowdrift events occurring. Even if most studies emphasize the importance of wind speed, as the frequency of snowdrift events increases with increasing wind speed, also snow characteristics, temperature, as well as liquid and solid precipitation are important (Amory, 2020; Arioli et al., 2023; Sturm et al., 2001; Zhang et al., 2022). Therefore, a correlation analysis with only one parameter is insufficient. Instead, I tested how multiple parameters behaved during snowdrift events versus during no snowdrift events. Additionally, I analyzed the variability of snowdrift events visually with a timeline of identified events. I performed the entire analysis and the creation of figures in the programming language R (version 4.3.3).

2.6 Validation of snowdrift events

I analyzed the webcam recordings visually to validate snowdrift events. Therefore, blowing snow had to be visible by eye. The detection is easier when the event intensity is higher which can happen at colder temperatures, because snow has a different crystal structure and can be lifted easier or at higher wind speeds. This also applies to old snow if the temperature is far below 0 °C, because older snow particles are rounder and have no clear crystal structure anymore (Baggaley & Hanesiak, 2005). This leads to the problem that especially big snowdrift events can be detected visibly, I could overlook smaller events.

To keep the bias as low as possible, I analyzed two cameras at Bayelva station for each event. If I clearly saw horizontal snow transport, I confirmed the event. If not, I subdivided the event into the following groups based on why I could not see snowdrift:

- rain/ snowfall, if I can see particle transport, but it is not clearly horizontal,
- fog,
- no visible snowfall due to light conditions, e.g. it is too bright or too dark and
- no image due to a snow-covered camera lens.

I followed this classification with all events and divided them whether both cameras lead to the same classification or whether I choose a different category between the cameras for the same event. I selected the validation image for the time in which the maximum snow transport was measured during each event. Nevertheless, I also had to account for a temporal mismatch between the camera and the maximum measured snow flux, as the camera captured an image every full hour, but the snow flux is averaged over a 30-minute period. Therefore, it is possible that the maximum snow flux of an event happened between two images. In this case, I always took the first image, so half an hour before the maximum snow flux was measured, because the snowdrift event is initiated at this time.

3 Results

3.1 Overview of data and flagging summary

The results of my flagging routine suit the data of the measured snow flux as over 95% were classified as good and just 4.8% had to be excluded because of plausibility (Figure 1). The flag 6 for plausibility is not a malfunction of the device as they measured rain events, but I excluded them because I focus on snowdrift events in this thesis. The remaining proportion (around 0.1%) is excluded due to maintenance, NA or physical limits. Therefore, the snow flux data is well suited to identify and analyze snowdrift events. However, the wind measurements of the FC4 sensor are not applicable, because just around 1.5% of the data is good and over 94% have decreased accuracy, even though I already applied a wide range for accuracy. In consequence, I used the quality-controlled meteorological wind speed.

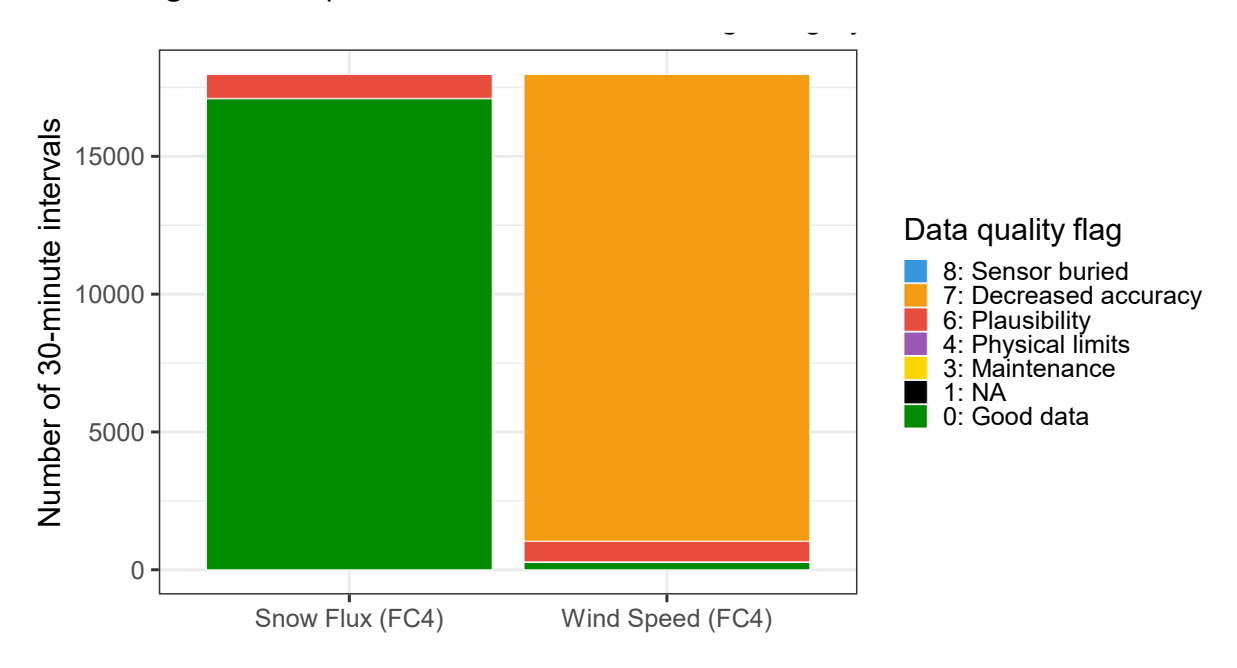


Figure 1: Summary of quality flags for the quality-controlled data from the FC4 sensor with flags from 0-8, except flag 2 (system error) and 5 (gradient) as the data was not flagged for these.

Also, the temporal distribution of the erroneous flags confirms that my flagging routine suits the dataset (Figure 2) and matches the meteorological data (Figure 3). I identified all rain events correctly, as they were flagged every time the tipping bucket measured liquid precipitation and the temperature rose above 0°C. Rain events mostly occurred in the summer, even if a few also happened in February and in the early period of the growing snow cover from September to November.

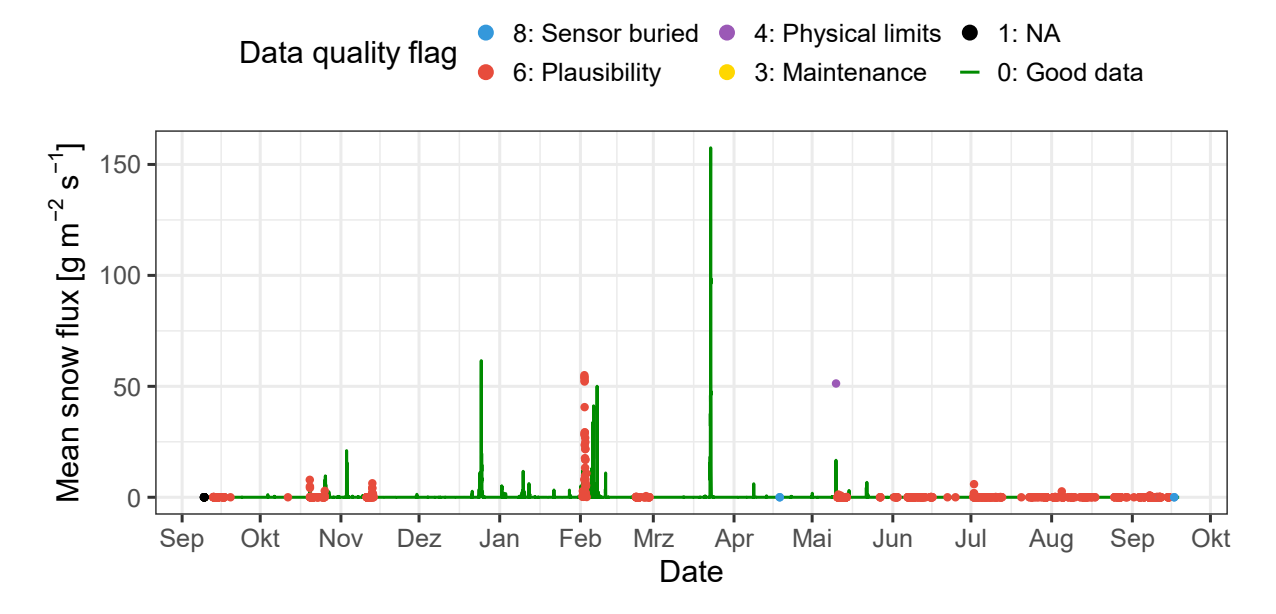


Figure 2: Times series of the 30-minutes mean snow flux measured by the FC4 sensor with applied quality control flags. The green line represents good data, whereas the points represent the erroneous quality flags in their specific color.

The meteorological parameters wind speed, temperature, precipitation and the characteristics of the snow with snow depth and density (b-e, from Figure 3) determine the occurrence and intensity of snowdrift events (a). The maximum wind speed is the primary driver of snowdrift, as the threshold for snow erosion must be reached for a snowdrift first (Figure 3b). Solid precipitation determines the availability of snow (Figure 3c). Especially from December to February snowdrift events often occur after the weighing precipitation gauge detects fresh snow. The temperature ranges from a minimum of over -24°C in March to a maximum of over 16°C in August, whereas the mean temperature of the analysis period is around -3°C (Figure 3d). However, the seasonal pattern is more mixed, with warm air interruptions in February and March which cause liquid precipitation (Figure 3c). This results in a change of the snowpack that is compacted by intermittent rain, while its depth decreases due to melting. The formation of the snowpack began in late September and ended in June with the beginning of the snow melt phase. The snow density increases throughout the season, which results in less snowdrift which can be seen in November and December as well as in late February and March (Figure 3a).

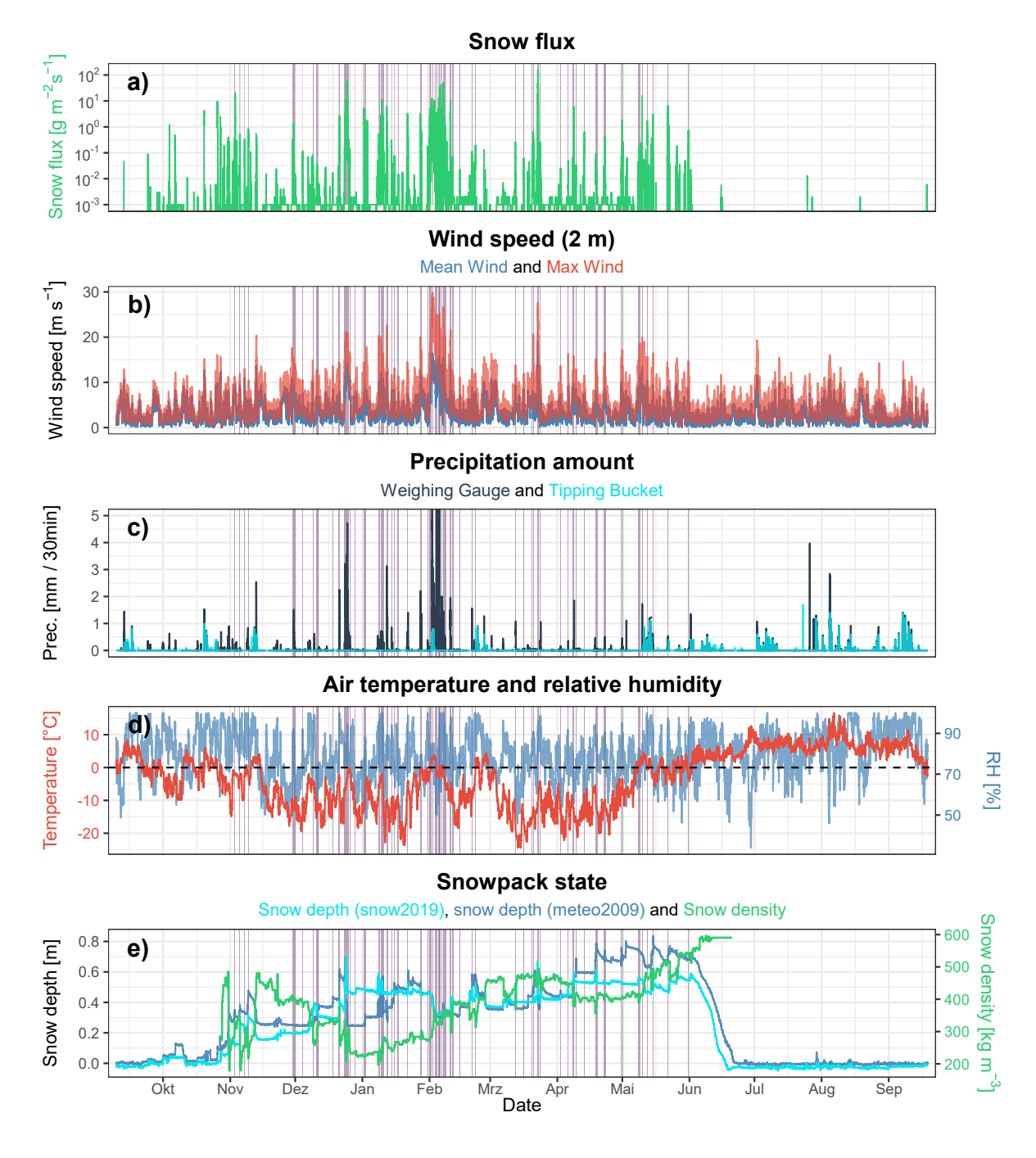


Figure 3: Overview of quality-controlled (just flag 0) parameters for the analysis from September 24 – September 25. The shaded light purple areas indicate my identified snowdrift events. With 30-minutes averages of a) mean snow flux (with logarithmic scale for better visibility of small events), b) mean and maximum wind speed, c) liquid (tipping bucket) as well as liquid and solid precipitation (weighing gauge) and d) air temperature and relative humidity. Along with the snowpack state in e) with the 30-miuntes average of the snow depth at the meteo station and the 1-hour average of the snow depth as well as the 6-hours average of snow density at the BaSnow2019 station.

3.2 Model performance

I calibrated the erosion efficiency e_{salt} by minimizing the MAE in comparison to the measured erosion derived from snow depth change (Figure 4). The MAE has a minimum error of 0.4 g m⁻² s⁻¹ which results in a erosion efficiency e_{salt} of 0.00035. The erosion efficiency would be twice as high with the RMSE.

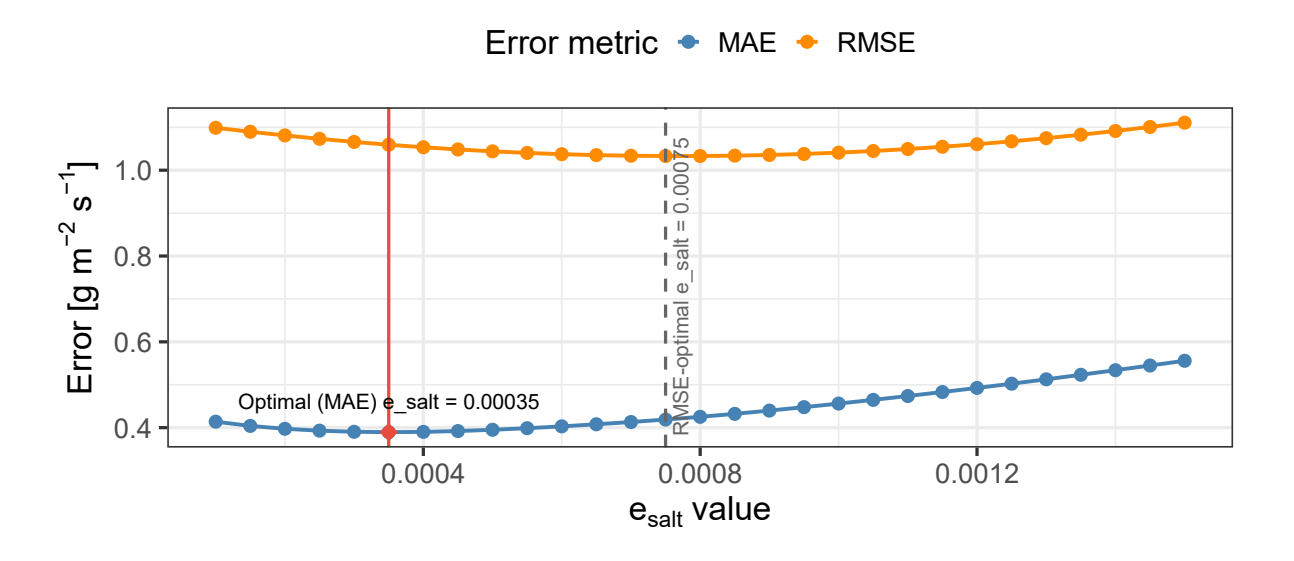


Figure 4: Calibration of erosion efficiency e_salt by finding the lowest MAE which is compared to the RMSE. The errors compare the data between the modeled erosion to the reference of measured erosion derived from snow depth change.

Nevertheless, the calibrated erosion flux underestimated the frequency as well as the intensity compared to the measured reference of erosion derived from negative snow depth change (Figure 5). The model predicts a very smooth erosion flux with a maximum spike of 1 g m⁻² s⁻¹ during the greatest snowdrift event in March. This clearly does not reflect the observed reality in which the spikes for the erosion flux have a great range with a maximum of over 15 g m⁻² s⁻¹. In addition, the frequency has a weak match with a spearman correlation of 0.39 for the modeled erosion compared to the derived erosion from both the meteo and the snow2019 station.

Derived erosion (met2009 station) — Derived erosion (snow2019 station) — Modeled erosion (mean wind)

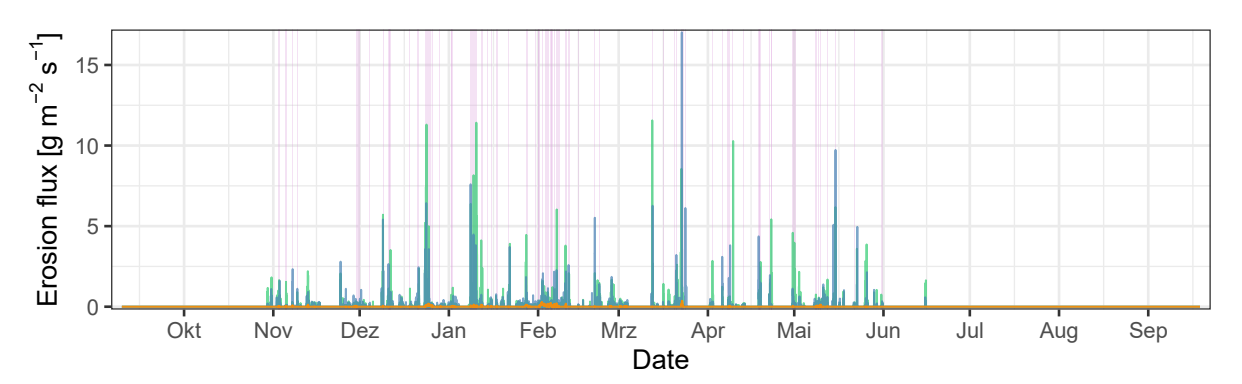


Figure 5: Time series of model performance with the modeled erosion flux (yellow), compared against the erosion derived from negative snow depth change for meteorological station (green) and snow2019 station (blue) from September 2024 to September 2025. The shaded light purple areas represent the identified snowdrift events.

I also built an alternative model using maximum wind speed instead of mean wind speed to see if this could better predict the peaks (Figure 6). This modification improved the Spearman correlation for the event frequency between the modeled and observed erosion, with values increasing to 0.70 for the snow2019 station and to 0.64 for the meteorological station. However, the predicted intensity of the events remained highly underestimated as the maximum spike of the modeled erosion just increased slightly to around $1.5~{\rm g~m^{-2}~s^{-1}}$.

Spearman ρ (model max vs snow2019): 0.71 | Spearman ρ (model max vs met2009): 0.65 Spearman ρ (Model mean vs snow2019): 0.39 | Spearman ρ (model mean vs met2009): 0.39

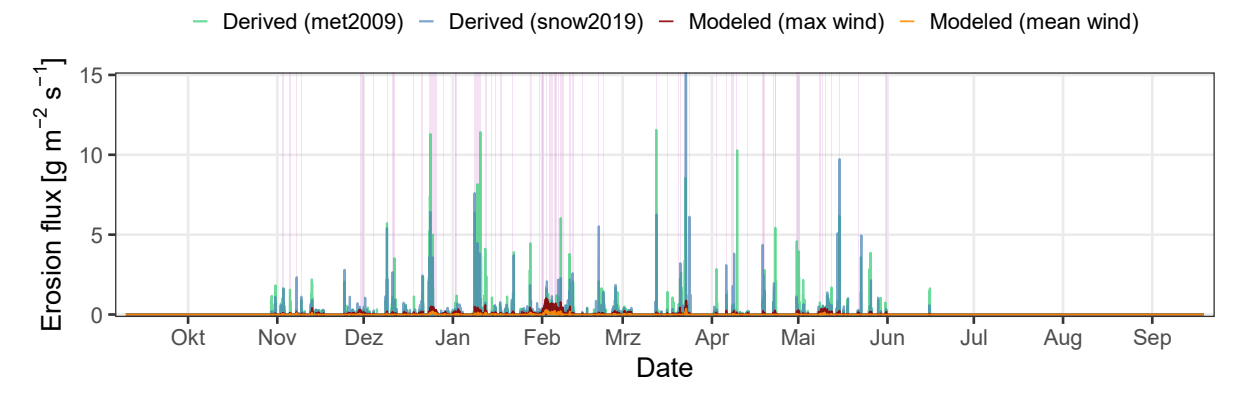


Figure 6: Time series of model performance with the modeled erosion flux from maximum wind speed (red) and from mean wind speed (orange), compared against the erosion derived from negative snow depth change for meteorological station (green) and snow2019 station (blue) from September 2024 to September 2025. The shaded light purple areas represent the identified snowdrift events.

3.3 Characterization of identified snowdrift events

I identified 73 snowdrift events in total that met all criteria that I applied. However, the snowdrift events were all very different in their snow flux intensity, meteorological parameters, snow characteristics and duration (Table 3). Therefore, I examined in which characteristics they differ from each other and in which parts they have similarities.

Table 3: Statistics of all 73 identified snowdrift events during the season from September 2024 to September 2025. All parameters are calculated for each event and rounded with their range, mean and median.

Measurement category	Observed range	Mean	Median
Snow flux max [g m^{-2} s ⁻¹]	0 to 345	30.1	2.4
Snow flux mean [g $\mathrm{m}^{-2}\ \mathrm{s}^{-1}$]	0 to 37.4	1.2	0.1
TST [kg m ⁻¹]	0 to 2290	61.2	2.3
Duration [hours]	3 to 52	8	6.5
Wind speed max in 2m [m s ⁻¹]	9.0 to 29.8	15.7	14.5
Wind speed mean in $2m [m \ s^{-1}]$	4.0 to 15.5	7.6	7.0
Air temperature in 2m [°C]	-18.0 to 3.2	-6.7	-7.5
Meteo station:			
Δ Snow depth <u>change</u> [m]	-0.30 to 0.15	0	0
Snow erosion <u>sum</u> [m]	0 to 1.20	0.08	0
Snow erosion max [m]	0 to 0.10	0.01	0
Snow deposition <u>sum</u> [m]	0 to 0.60	0.08	0
Snow deposition max [m]	0 to 0.30	0.02	0
Snow2019 station:			
Δ Snow depth <u>change</u> [m]	-0.09 to 0.15	0	0
Snow erosion <u>sum</u> [m]	0 to 0.80	0.07	0
Snow erosion max [m]	0 to 0.10	0.01	0
Snow deposition <u>sum</u> [m]	0 to 1.10	0.07	0
Snow deposition max [m]	0 to 0.20	0.02	0
SWE [mm]	38.3 – 296.5	147.2	127.0

3.3.1 Snow flux

My analysis revealed that snow transport is dominated by a few high-intensity events, which raise the average for snow flux and total transported snow (TST). The events not just differ from each other, but also in themselves as the mean and maximum fluxes have a great variety through single events (Table 3). For example, the maximum snow flux ranges from 0 to 345 g m $^{-2}$ s $^{-1}$ with an average of around 30 g m $^{-2}$ s $^{-1}$ and the median just around 2 g m $^{-2}$ s $^{-1}$. This shows that half of all events have a very low intensity with a

maximum snow flux below $2~g~m^{-2}~s^{-1}$. In comparison, the mean snow flux for all events has a range from just 0 to 37 g m $^{-2}~s^{-1}$ with a mean value around 1.2 g m $^{-2}~s^{-1}$ and the median is 0.1 g m $^{-2}~s^{-1}$. Interestingly, in both the mean and max flux the statistical mean within this category is around 12 times bigger than the median. This same pattern is even more pronounced in TST. In this, the mean of 61.2 kg m $^{-1}$ is over 26 times greater than the median with 2.3 kg m $^{-1}$. This indicates that events with a higher mean flux also have a longer duration. However, I cannot see a relationship between duration and intensity in the distribution of events (Figure 7). Nevertheless, the duration also has a very wide range from 3 hours (which was the minimum threshold) up to 52 hours, whereas the mean duration is with 8 hours higher than the median with 6.5 hours. This indicates that half of the events lasted relatively short.

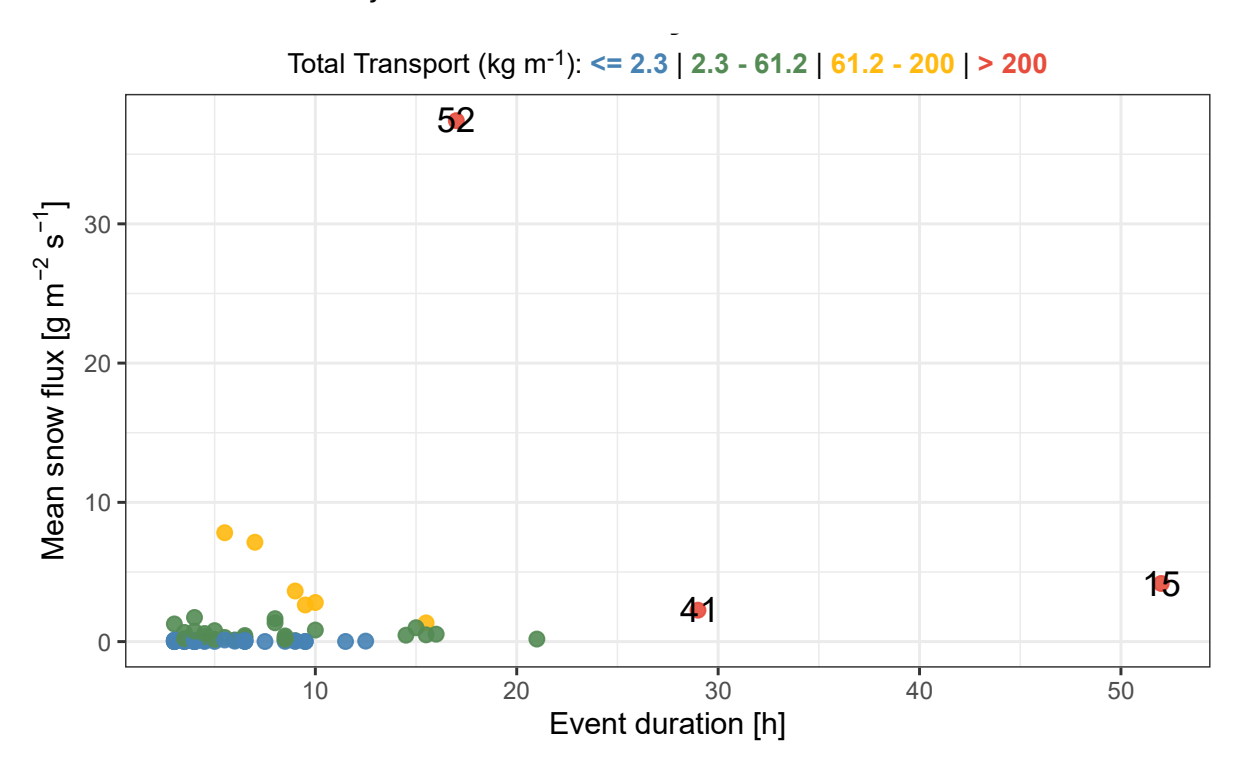


Figure 7: Distribution of identified events in the season from September 2024 to September 2025 with mean flux and event duration grouped by their TST. Each point is one event with their mean flux averaged over the event and their duration. The highest TST category is labeled with the ID of the events (15, 41, 52).

3.3.2 Wind speed and direction

While wind speed is the primary driver of snowdrift, it is not the sole factor as the snow conditions are also important. Figure 8 supports this by comparing all 30-minute intervals of snowdrift events to periods when no snowdrift occurred, even though the wind speed passed the threshold. The median of the maximum wind speed during snowdrift intervals is around 2 m s⁻¹ higher at 12 m s⁻¹ compared to periods when no snowdrift occurred. While both categories contain many outliers above 1.5 times the interquartile range (IQR), outliers are more frequent and extreme during snowdrift events and reach almost 30

m $\rm s^{-1}$. This confirms that higher wind speeds strongly correlate with the occurrence of snowdrift events (Figure 8). However, the summary characteristics of the events as a whole have higher mean and median values (Table 3). For example, the mean peak wind speed across all events is 15.7 m $\rm \, s^{-1}$, whereas the median is 14.5 m $\rm \, s^{-1}$. This highlights that there is a great variability in intensity between single events (Table 3). Furthermore, the maximum wind speed is nearly twice as high as the average wind speed across the events in all statistics (range, median and mean). This indicates that in most events shorter gusts of wind are responsible for snowdrift to pass the erosion threshold.

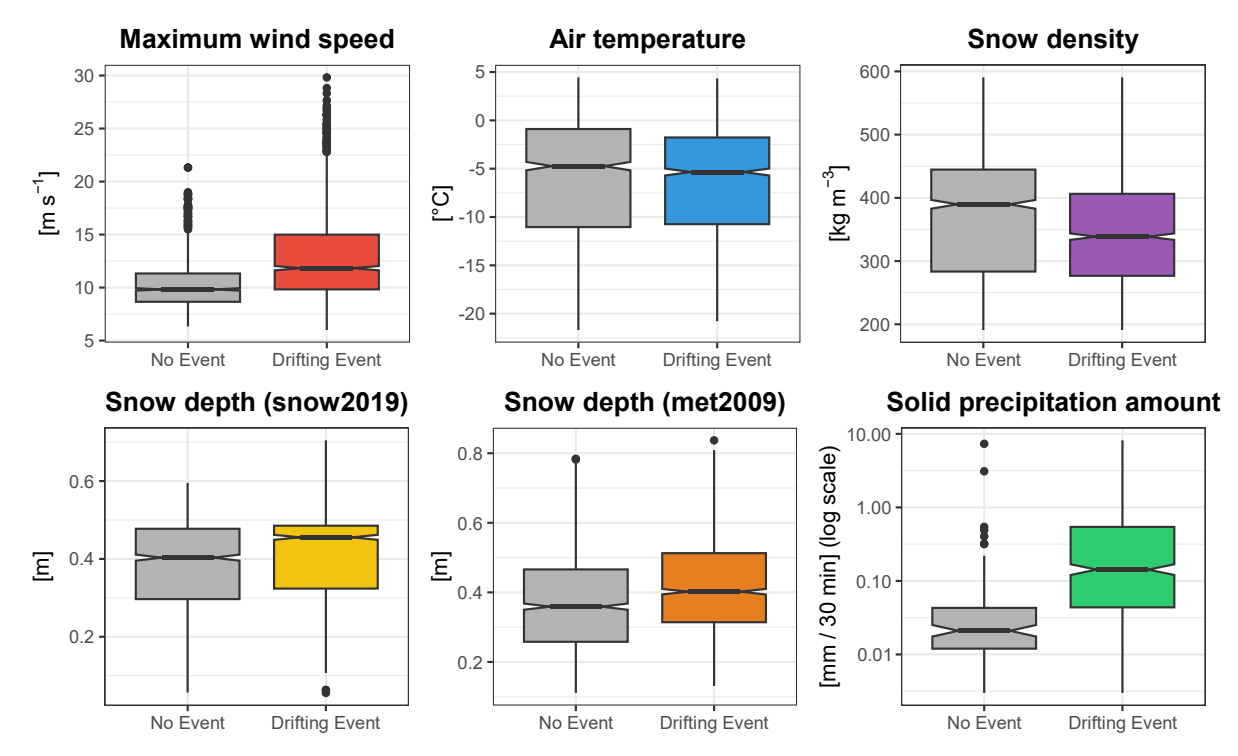


Figure 8: Comparison of environmental conditions during each 30-minutes interval of identified snowdrift events versus non-events. No-event periods are restricted to periods in which all preconditions for a potential snowdrift event are fulfilled (no rain and wind speed threshold was passed), but no snowdrift occurred. The box plot shows the median (center line) with the 95% confidence interval (indentation around the median), IQR (box) and the whiskers that extend to 1.5 times of the IQR. Points beyond the whiskers are outliners. *Note: Median values differ from Table 3 as the figure includes all 30-minutes periods during identified events and not just the averages of each event.*

The dominant wind direction during snowdrift events is from East-Southeast (ESE) and contributes to nearly 60% of the mean snow flux (Figure 9a). The erosion and accumulation of snow differ due to the location of the snow depth measurement station (Table 3). In sum, more snow accumulates at the BaSnow2019 station, which is located on the leeward side, directly behind the corner of the fence (Figure 9b). In contrast, more snow erodes at the BaMet2009 station in sum, which is also located on the leeward side of the fence but further away than the snow station.

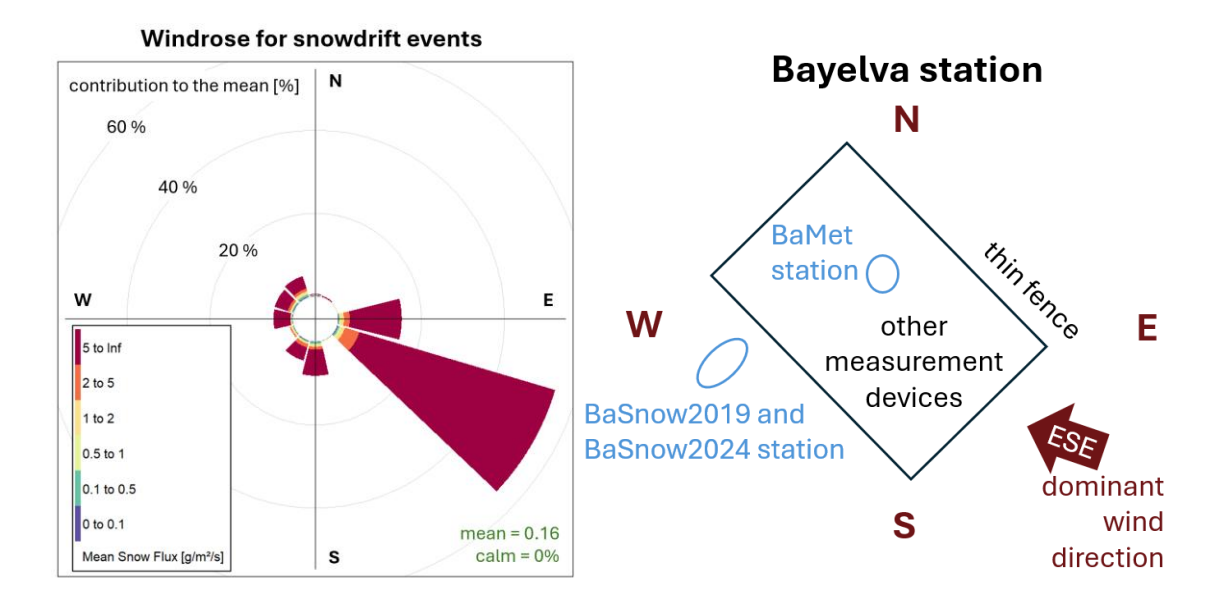


Figure 9: (a) Wind rose at meteorological station shows dominant wind directions during snowdrift events grouped by mean flux intensity (colors). Beams represent the direction from which the wind blows, whereas the length of the beams indicate the contribution to the mean snow flux in [%]. (b) Schematic illustration for an overview of the sensors locations and cardinal directions at Bayelva station. This is based on the topographic map for Bayelva station (Norwegian Polar Institute, 2025).

3.3.3 Snow characteristics

The data reveals a clear relationship between snow density and the occurrence of snowdrift events. While events occur at medium to lower snow density with a median around 340 kg $\,\mathrm{m}^{-3}$, non-events have a higher median density around 390 kg $\,\mathrm{m}^{-3}$ (Figure 8). This pattern is also visible in Figure 10, where the highest snow flux is associated with mostly light to medium density. Nevertheless, there are still some intervals in which the density was high, but a very high snow flux was measured (Figure 10).

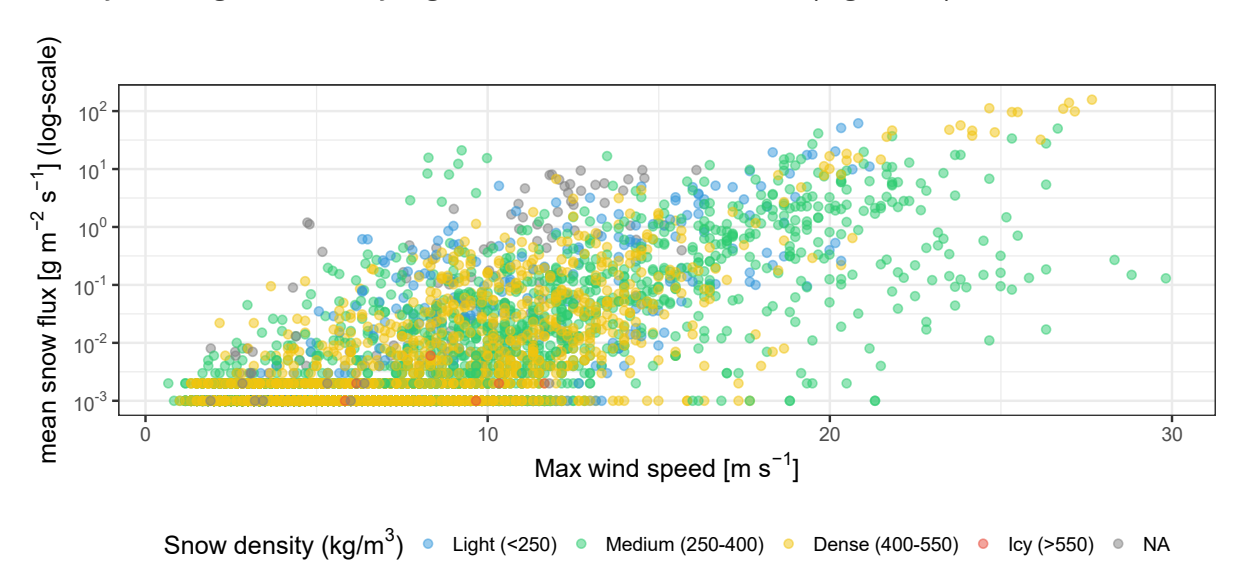


Figure 10: The relationship between maximum wind speed and mean snow flux (logarithmic scale) for all 30-minutes intervals where snow flux was measured (snow flux > 0). Each

measured snow transport is represented by one point and colored by snow density. The snow density for grey data points is NA.

The snow accumulation period starts in late September (Figure 11). From there on the snowpack constantly increases as the SWE ranges from 38 to 397 mm (Table 3). The thawing period begins in June and proceeds rapidly within two weeks (Figure 11). In February a discrepance occurs between the high amount of solid precipitation that is measured while the SWE barely increases (Figure 11a).

When I compare the snow depth change between the two different stations (BaMet2009 and BaSnow2019), I can see differences in snow redistribution on a micro scale. While the average of the snow depth net change is balanced and remains zero for both stations, the range of the meteorological station shows that more snow erodes as it ranges from -0.30 to 0.15 m unlike the snow2019 station with a range from -0.09 to 0.15 m. This is also reflected in the behavior of the snow depth change, as more snow erodes in sum at the meteorological station, whereas at the snow2019 station more snow accumulates in sum. Overall, this clarifies that the meteorological station is more exposed to wind. Nevertheless, the low maximum and mean values for erosion and deposition in comparison to the total erosion and deposition indicate that during most snowdrift events the periods of erosion and accumulation are fluctuating and the snow depth changes steadily during an event (Figure 11b).

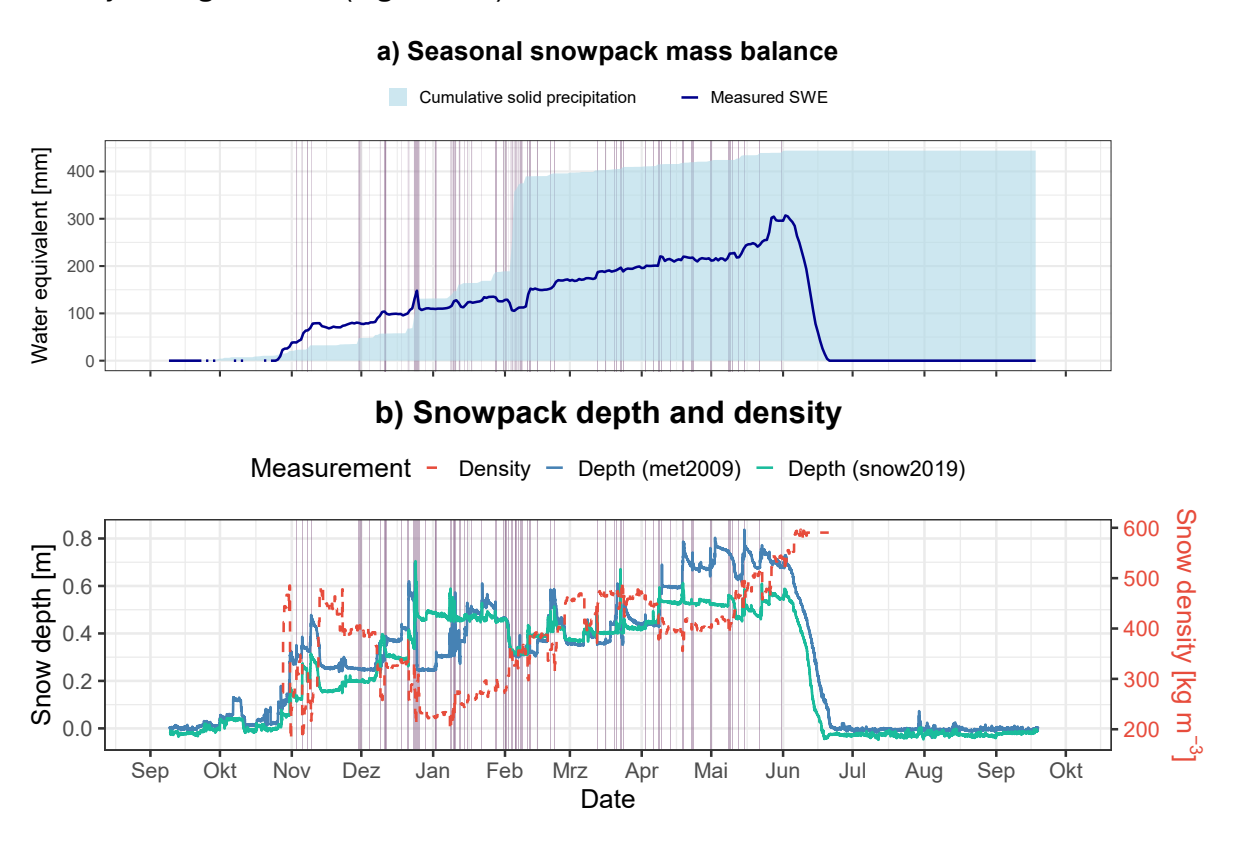


Figure 11: Time series from September 2024 to September 2025 for the snowpack state with a) daily mean values of the snow water equivalent and the cumulative sum of the daily solid precipitation and b) 30-minutes averages of snow depth from meteo station as well as 1-hour

averages of snow depth from snow2019 station and the calculated 6-hourly snow density. The shaded light purple areas indicate the observed snowdrift events.

3.3.4 Air temperature

Air temperature had a great variety during snowdrift events with a range from -18 to 3.2 °C, while the mean value is at -6.7 °C and the median slightly lower at -7.5 °C (Table 3). While temperatures during events versus non-events are very similar, the IQR is slightly lower during snowdrift events (Figure 8). Interestingly, Figure 12 shows that for the same wind speed, the mean snow flux is higher in moderate temperatures from -13 to +1 °C (Figure 12). Also with lower wind speed, between 4 to 10 m s $^{-1}$, the average snow flux is higher at temperatures between 0 to 5 °C than for example up to -18 °C.

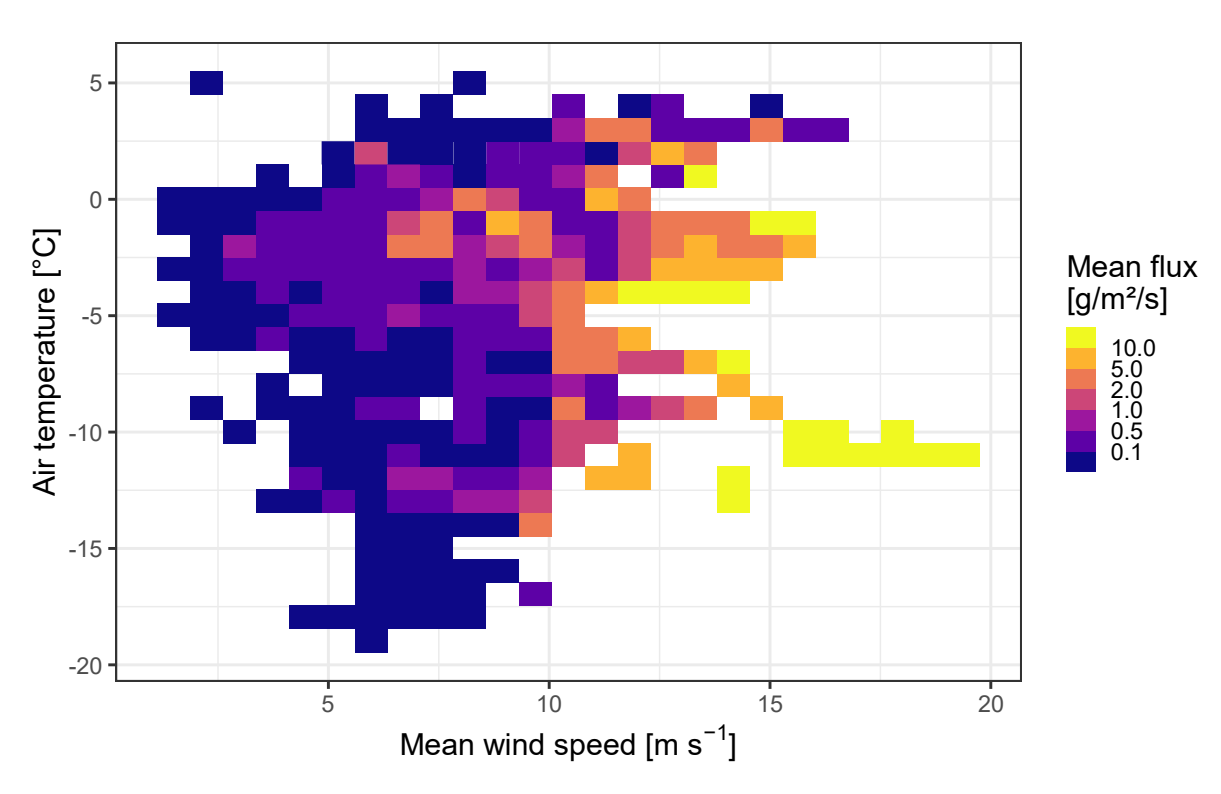


Figure 12: The relationship between air temperature at 2 m height [°C] and mean wind speed at 2 m [m s $^{-1}$], grouped by the mean snow flux [g m $^{-2}$ s $^{-1}$] averaged over all 30-minute measurement intervals during snowdrift events in the period between September 2024 to September 2025.

3.3.5 Precipitation

The occurrence of snowdrift events increases with solid precipitation. The mean solid precipitation for non-events is around 0.03 mm, while the mean during snowdrift events is much higher at around 0.2 mm (Figure 8). Furthermore, solid precipitation events with at least 0.5 mm of snow water equivalent increase the occurrence of snowdrift events by more than 30% on the same day (Figure 13). Contrary, the probability of a snowdrift event

together with liquid precipitation is much lower and does not exceed 8% even in the following 14 days.

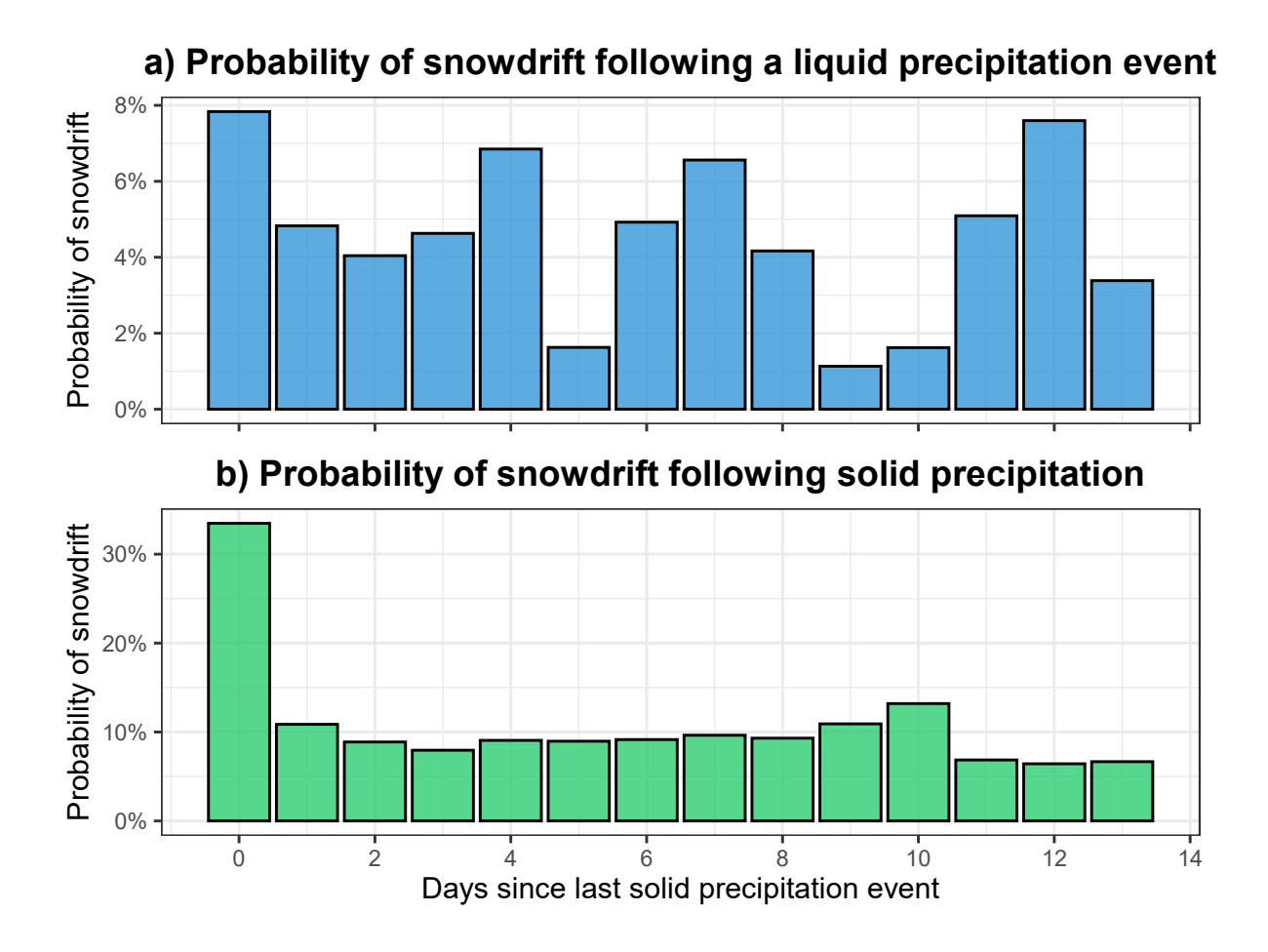


Figure 13: Propability of the occurence of snowdrift events [%] following a) a liquid precipitation event of b) a solid precipitation event by the number of days since the last important precipitation event (at least 0.5 mm).

3.4 Detailed analysis of snowdrift events

I analyzed four snowdrift events in detail. I selected the most different events as possible to represent different snow characteristics and drivers that initiate the event. I selected them by these criteria:

- event 1 represents a very early season event,
- event 34 had the highest temperature across the events and is directly surrounded by two rain events,
- event 52 had the highest TST and
- event 73 represents the last event during the snowdrift season and has the highest snow density.

The early season event 1 in November is remarkable, because the snow flux is relatively low in the beginning and suddenly increases as soon as solid precipitation occurs (Figure

14). The maximum wind speed occurred at 11 p.m. with 11 m s⁻¹ and decreased afterwards with some fluctuations. At the peak of wind speed, the snow flux was very low, staying under $10 \, \mathrm{g \, m^{-2} \, s^{-1}}$, mostly even under $1 \, \mathrm{g \, m^{-2} \, s^{-1}}$. Four hours after the peak wind speed, the snow flux suddenly rised up to $125 \, \mathrm{g \, m^{-2} \, s^{-1}}$. The snow depth was around 30 centimeters at the meteorological station and 12 centimeters at the snow2019 station. The snowdrift ceased together with decreasing snowfall as well as declining wind speed.

Event 34 in February took place under the highest temperature across all identified snowdrift events (Figure 15). Additionally, it occurred right after a rain event. To get a better overview, I plotted an additional interval in the end to examine the snowdrift as soon as rain started. The tipping bucket measured an amount of 0.2mm rain per 30 minutes during the last interval. Interestingly, this did not change the snow characteristics to prevent snowdrift. Conversely, the snow depth increased during the last interval. Even if the temperature is relatively high and ranges from 2.8 to 3.4 °C, the density stays constant at 306 kg m⁻³ throughout the whole period. Also, the wind speed is high with a maximum around 30 m s⁻¹ and stays high over the whole period with at least 22 m s⁻¹ for the maximum and 12 m s⁻¹ for the mean wind speed.

The major snowdrift event 52 with the highest TST occurred in March and consists of both: a long duration and a high snow flux (Figure 16). It was the 4th longest event with a duration of 17 hours and had the highest maximum snow flux with 345 g m⁻² s⁻¹ resulting in a TST of around 2290 kg m $^{-1}$. With a density of 446 kg m $^{-3}$ during the largest snow transport, this results in a transported volume of over 5 cubic meters per meter of transported snow during the event $(2290 [\text{kg m}^{-1}] : 446 [\text{kg m}^{-3}] = 5.1 [\text{m}^3 \text{ m}^{-1}])$. The wind speed followed the same pattern as the snow flux starting 17 m $\rm s^{-1}$, then increased to nearly 28 ${\rm m~s^{-1}}$ and dropped to 7 ${\rm m~s^{-1}}$ in the end of the event. Furthermore, a steady increase in snow drift is visible throughout the entire event, as well as an equally steady decrease after the peak at 7 hours after initiation. The snow depth is above 40 centimeters for both sensors. Interestingly, the main change in snow depth happened before the peak of the snow flux. The sensor at the snow2019 station first measured deposition and 3 hours later erosion, both of nearly 25 centimeter. The snow depth at the meteorological station slowly decreased of about 10 centimeters during the first 2 hours. No notable snow depth change was measured during and after the snow flux peak. At the highest peak, the temperature is around -11 °C and increased throughout the event from nearly -13 to -7°C.

The last snowdrift event 73 occurred in late May and is characterized by a big and dense snowpack (Figure 17). While the snow depth ranges from 55 cm for the meteorological and 67 cm for the snow2019 station, the density is very high with 541 kg m⁻³. Furthermore, the wind speed was relatively low, with a maximum around 15 m s⁻¹ and a mean of 7 m s⁻¹. The snowdrift increased with the beginning of solid precipitation. The temperature during the event decreased from -1.5 to -3.2 °C.

During all events, the relative humidity increased as soon as snowdrift occurred by between 5 to 10%.

Snow flux Flux measurement — Max — Mean — Min a) $Flux [g m^{-2} s^{-1}]$ 100 50 Wind speed Wind measurement - Max - Mean Wind speed [m s⁻¹] b) 10 9 8 **Precipitation amount** Precipitation [mm] C) 0.20 0.15 0.10 0.05 0.00 Air temperature and relative humidity Measurement - RH 2m - Temp 2m Air temperature [°C] Rel. humidity [%] -2.0 92 Snow depth and density Measurement - Density Depth (met2009) — Depth (snow2019) Snow density [kg m⁻²] 0.35 e) Snow depth [m] 0.30 0.25

Detailed analysis of snowdrift event 1 Start: 02-11-2024 21:30 | Duration: 9 h | TST: 117.7 kg/m

Figure 14: Quality-controlled parameters during early-season snowdrift event 1 on November 2-3, 2024. The parameters are the 30-minutes averages of a) min, mean and max snow flux, b) mean and max wind speed, c) amount of solid precipitation from the weighing precipitation gauge (liquid precipitation is excluded due to the rain threshold for snowdrift events) and d) air temperature and relative humidity. Panel e) shows the 30-minutes averaged snow depth at the meteo station and 1-hour averaged snow depth at snow2019 station as well as 6-hour averages of snow density.

Time

07:00

03:00

0.20 0.15

23:00

Results 26

05:00

Special analysis of snowdrift event 34

Start: 02-02-2025 08:30 | Duration: 3 h | TST: 13.7 kg/m

Snow flux (unfiltered)

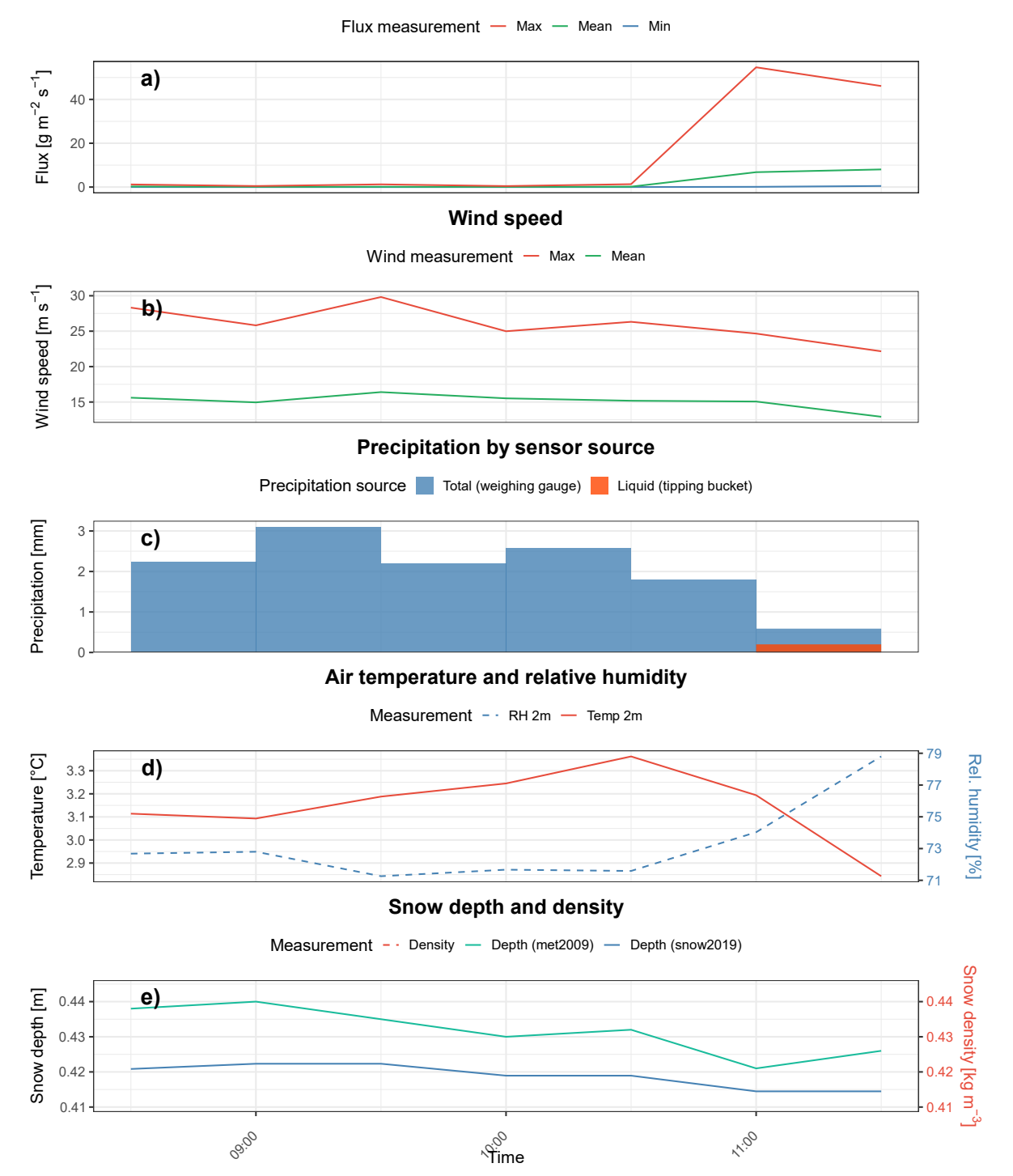


Figure 15: Parameters during event 34 with highest temperature on February, 2, 2025. The values for a) min, mean and max snow flux are raw data as the original last time step was flagged for plausibility, because it was interrupted by rain. The other parameters are good-data from quality assessment with the 30-minutes averages of b) mean and max wind speed, c) amount of liquid and solid precipitation from weighing precipitation gauge and liquid precipitation from tipping bucket and d) air temperature and relative humidity. Panel e) shows the 30-minutes averaged snow depth at the meteo station and 1-hour averaged snow depth at snow2019 station. 6-hourly snow density can't be displayed, but is at 306 kg m $^{-3}$ over the whole event.

Detailed analysis of snowdrift event 52

Start: 22-03-2025 18:00 | Duration: 17 h | TST: 2289.6 kg/m

Snow flux

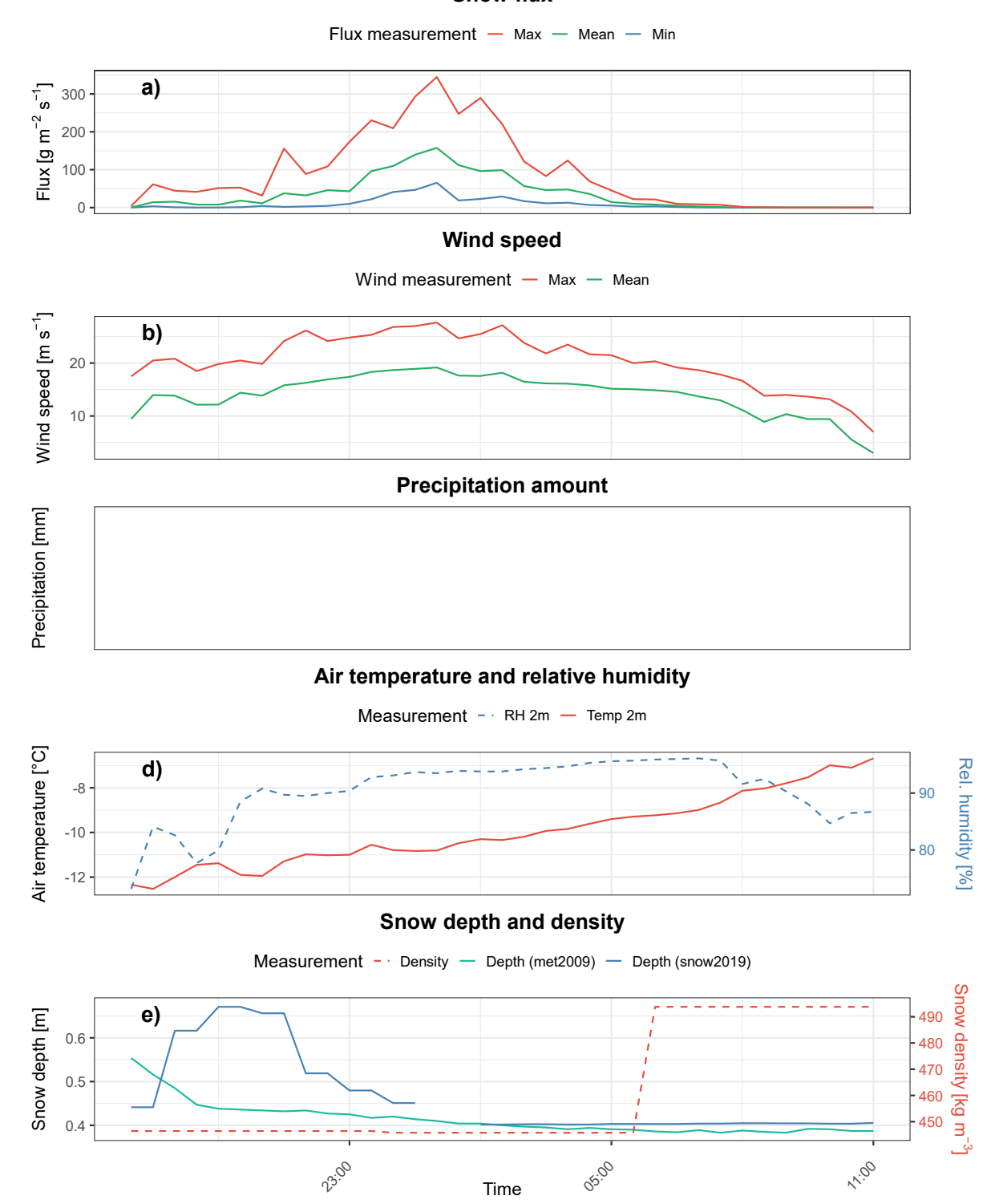


Figure 16: Quality-controlled parameters during snowdrift event 52 with highest TST on March 22, 2025. The parameters are the 30-minutes averages of a) min, mean and max snow flux, b) mean and max wind speed, c) no measured amount of solid precipitation from the weighing precipitation gauge (liquid precipitation is excluded due to the rain threshold for snowdrift events) and d) air temperature and relative humidity. Panel e) shows the 30-minutes averaged snow depth at the meteo station and 1-hour averaged snow depth at snow2019 station as well as 6-hour averages of snow density.

Detailed analysis of snowdrift event 73 Start: 31-05-2025 07:30 | Duration: 8.5 h | TST: 5.3 kg/m Snow flux

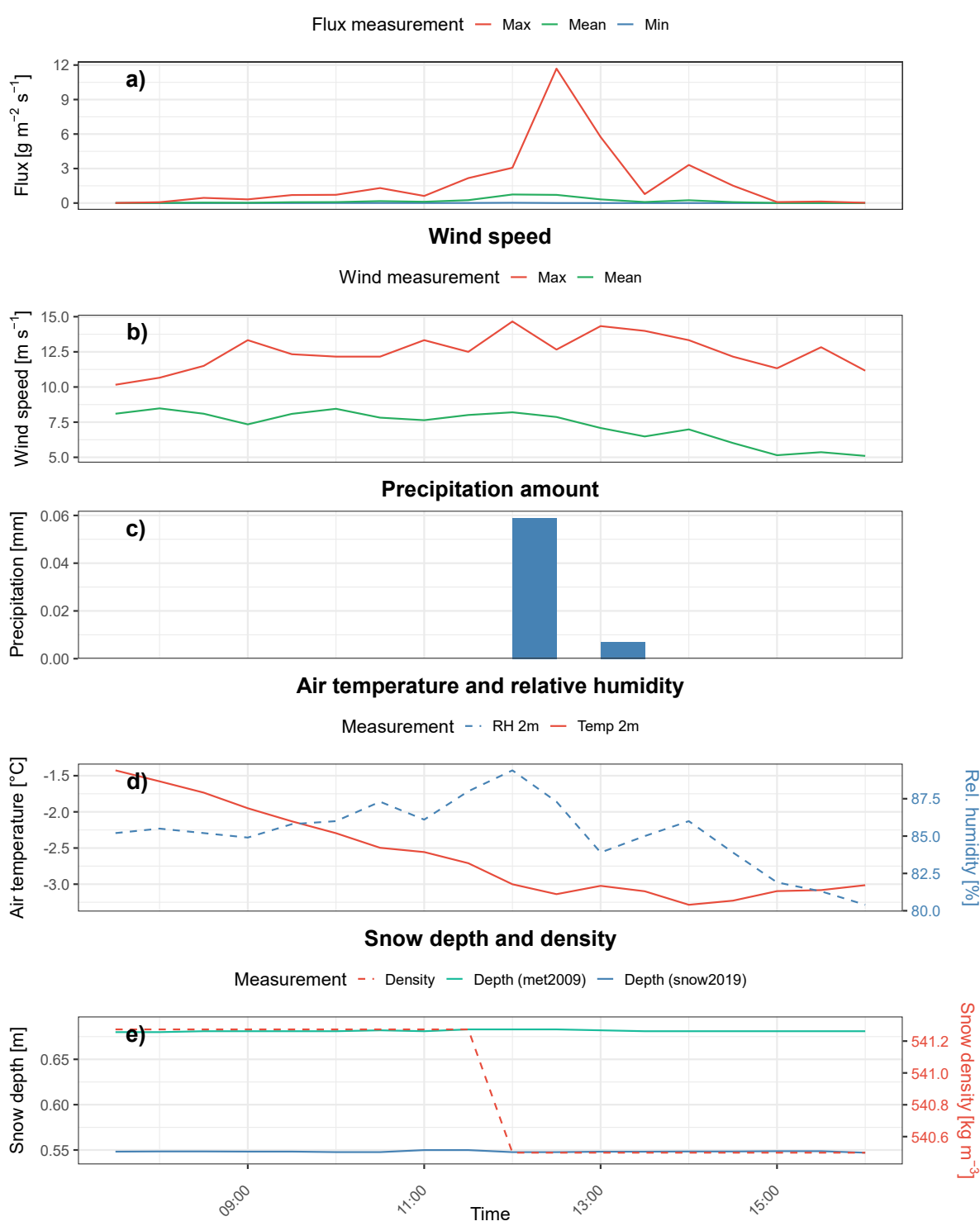


Figure 17: Quality-controlled parameters during late-season snowdrift event 73 with highest snow density on May 31, 2025. The parameters are the 30-minutes averages of a) min, mean and max snow flux, b) mean and max wind speed, c) amount of solid precipitation from the weighing precipitation gauge (liquid precipitation is excluded due to the rain threshold for snowdrift events) and d) air temperature and relative humidity. Panel e) shows the 30-minutes averaged snow depth at the meteo station and 1-hour averaged snow depth at snow2019 station as well as 6-hour averages of snow density.

3.5 Validation of snowdrift events

The validation showed that I could not clearly identify more than half of the events visually. From the matching classification between both cameras, I just confirmed 16 events which make up 22%, whereas I could not validate 52% of the snowdrift events (Table 4). The rest of the events differed in their classification between the cameras. When I count all events as validated in which I could point out snowdrift from at least one camera, the total amount of validated events is 42%.

Table 4: Classification of snowdrift events from visual validation with the two webcams BaCam1 and BaCam2. The event IDs are displayed in the "matching" column when the images from both cameras belong to the same group and if not, they are in the "divergent" column. The events are categorized for event (horizontal particle transport), rain/ snowfall (not clearly horizontal particle transport), fog, to bright/dark or no snowdrift visible or camera is snow covered.

validation category		matching	divergent	
		camera 1 and 2	Camera 1 Came	ra 2
assigned	event	1, 2, 4, 7, 8, 9, 11, 12, 13, 14, 21, 26, 32, 33, 41, 52	3, 22, 23, 24, 10, 39, 2 27, 28, 29, 34, 35, 37, 45, 59	13
not clear assignable due to	rain / snowfall	53	47	
	fog	25, 36, 42, 51, 60, 61, 63, 64, 66, 70, 71	23, 24, 2 37, 65	9, 35,
	too bright/dark or no snowdrift visible	16, 17, 18, 19, 20, 30, 31, 38, 44, 46, 48, 49, 50, 54, 55, 56, 57, 58, 62, 67, 68, 69, 73	10, 43, 65 3, 15, 2 28, 34, 3 45, 59	
	camera is snow covered	5, 6, 72	15, 39, 40 47	

4 Discussion

4.1 Model performance

The weak match between the modeled erosion and the reference of erosion derived from snow depth change showed that the model is not suitable for my dataset. This underestimation is partially a consequence of the calibrated e_{salt} value. Nevertheless, it was the right choice to use MAE instead of RMSE to calibrate the model as my data is not normally distributed and the events have a great range with outliers. Therefore, the low erosion efficiency indicates that the snowpack is very resistant to wind erosion. This erosion resistance is caused by the weather conditions at Bayelva station. There are frequent intrusions of warm air and warm winter storm events that bring rain This melts the snow and leads to an icy crust that is very hard to erode. Warmer temperatures also lead to sintering of snow which increases density. This results in a smooth modeled erosion flux that underestimated the events' intensity and frequency. I tried to improve this by modeling the maximum instead of the mean wind speed, as mostly the turbulent gusts are responsible for snow erosion (Stull, 1988). This model had minor improvements for the frequency, but still underestimated the intensity. This raises the question of whether a single, static e_{salt} value is sufficient as the snowpack changes throughout the whole season.

Another reason for the mismatch is that the model assumes the snow surface as straight line, but the reference erosion flux also measured snow forms. For example, sastrugi that drift through the snow depth measurement area are counted as erosion in my reference measurements. Sastrugi are wind-driven erosion forms that consist of wind-hardened snow and mainly have sharp edges from grooves or furrows (Filhol & Sturm, 2015). They are visible in the short-term spikes of snow depth (Figure18). As the snow depth is averaged for 30-minutes for the meteorological station and 1-hourly for the snow2019 station, sastrugi are better visible in drifting events with a long duration, even if they also occur in short events. The formation of sastrugi is also observed by other scientists in Svalbard (Ferrari et al., 2005; Haapala et al., 2013; Mäkiranta et al., 2011). However, sastrugi can't be counted as erosion, because they are a form of snow transport (Filhol & Sturm, 2015). Therefore, the reference I used to validate the model overestimates erosion as it counts sastrugi as erosion.



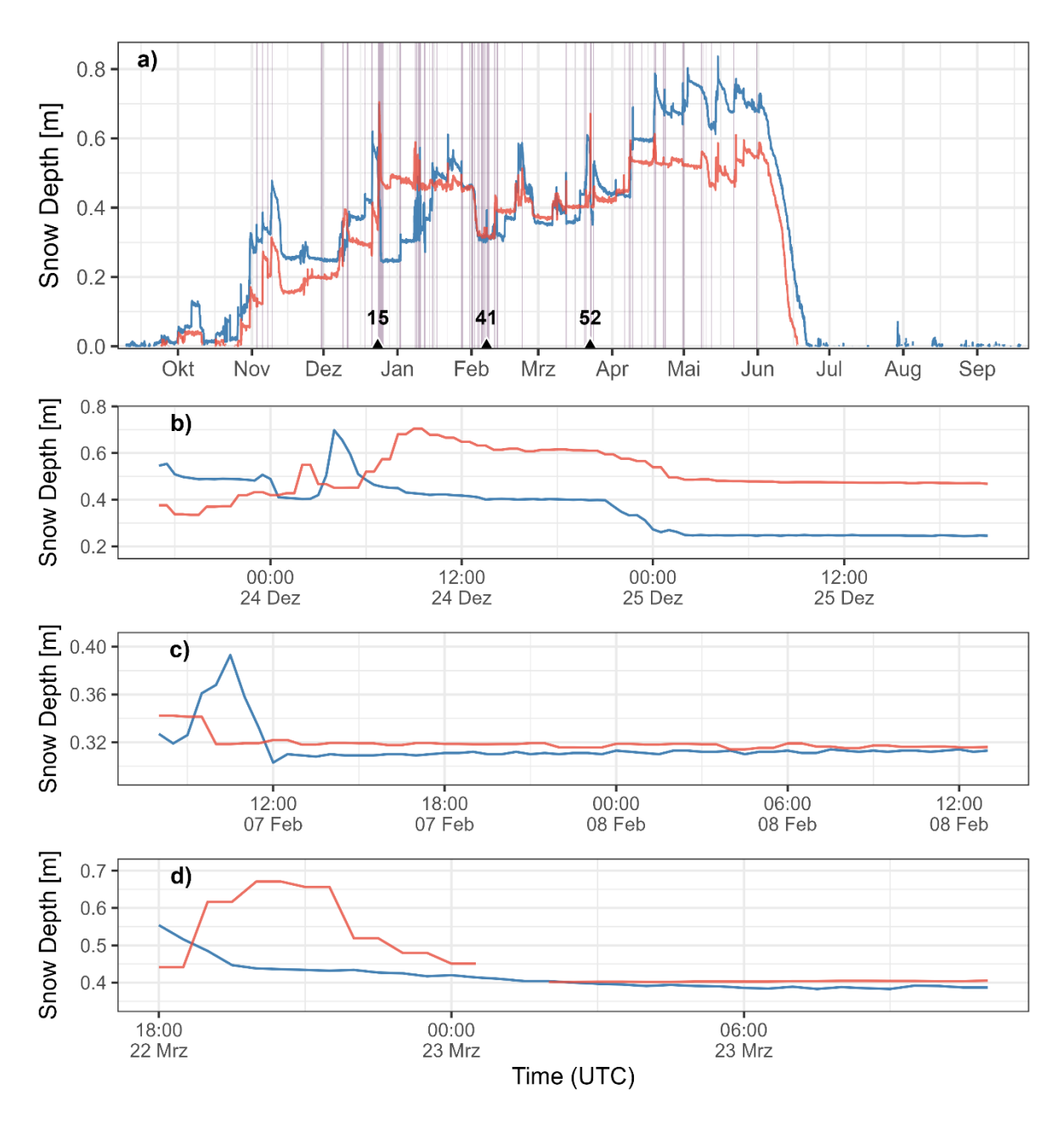


Figure 18: Analysis of snow depth from 30-miuntes averages of meteo station (blue) and 1-hour averages of snow2019 station (red) for sastrugi detection. Panel a) shows the seasonal overview from September 2024 to September 2025 with the identified snowdrift events (shaded vertical lines). The triangles show the events that are analyzed in detail below with ID 15 in b), ID 41 in c) and ID 52 in d).

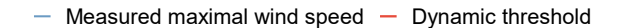
Additionally, the averaged values of snow density create a mismatch between the modeled erosion and erosion derived from snow depth change. The snow density is used for the calculations of the model, but it is calculated over the whole snowpack, whereas deeper layers in the snowpack mostly have a much higher density than layers on the top. One exception is depth hoar which can also occur during snowdrift events, building thin layers of hoar between snow crystals and underneath the snowpack with a very low density (Akitaya, 1973; Sturm et al., 2001). Nevertheless, snow crystals are compressed

by the layers above as well as by thawing-freezing cycles which lead to ice formation. Therefore, the entire snowpack typically has a higher density than the upper fresh snow. However, only the upper layer is eroded, so the calculations for erosion should use the much lower density of the surface layer. As this cannot be measured with the existing sensors, I could use a specified fixed value of light to medium dense snow. This would improve the model, particularly in late season which is underestimated in the current model (Figure 18).

Furthermore, the model simplifies complex wind systems and snow dynamics. For example, snow that is eroded leads to more erosion which is not taken into account. This process is called the "splash" effect (Naaim et al., 1998). The already eroded particles in the saltation layer can transfer energy with their impact and erode more particles in a chain reaction. Also, the wind pattern is more complex, with turbulent gusts that are just represented in one averaged value in the model, which cannot describe the wind dynamics sufficiently. Additionally, I used simplified calculations from the original model, therefore other processes like sublimation are also not accounted for in my modeled erosion flux (Sauter et al., 2013).

4.2 Suitability of thresholds

The dynamic wind speed threshold was meaningful, as it followed the same pattern of the snow density which limits erosion in the first place (Pomeroy & Gray, 1995). As the wind speed threshold is calculated from the density, it also increases during the season with fluctuations in the early accumulation period due to rain events. The threshold ranges from 5.7 m s⁻¹ in November to 10.1 m s⁻¹ in June with a mean at 8.7 m s⁻¹ and the median at 8.8 m s⁻¹ (Figure 20). Especially at the end of December and in January the wind speed threshold is close to the value of 6 m $\rm s^{-1}$ that was used in literature (Cierco et al., 2007). When the snow gets denser, the wind speed needs to be higher to erode snow particles and transport them at a height above 80 centimeters, therefore events also need a higher wind speed threshold. This method of a dynamic wind speed threshold is useful and is also used by other authors, as in reality there is no fixed wind speed threshold (Pomeroy & Gray, 2005). Nevertheless, a mean wind speed threshold of 8.7 m s⁻¹ is higher than most values I found in literature, for example around 6 $\rm m\,s^{-1}$ at Svalbard (Jaedicke & Gauer, 2005; Li & Pomeroy, 1997) and 6 m s⁻¹ for the French Alps (Cierco et al., 1998). However, it matches with the wind speed threshold of 10 m s⁻¹ found by Ovesen, but their study site is not comparable to Bayelva, as they placed the sensor on a hill, therefore this value is not representative (Ovesen, 2024). The reason for my increased wind speed threshold is that the threshold is biased by density, which is overestimated especially during late season, because the whole density of the snowpack is determined, even if just the lighter snow in the top layer is eroded. Therefore, the wind speed threshold is also overestimated especially during late season.



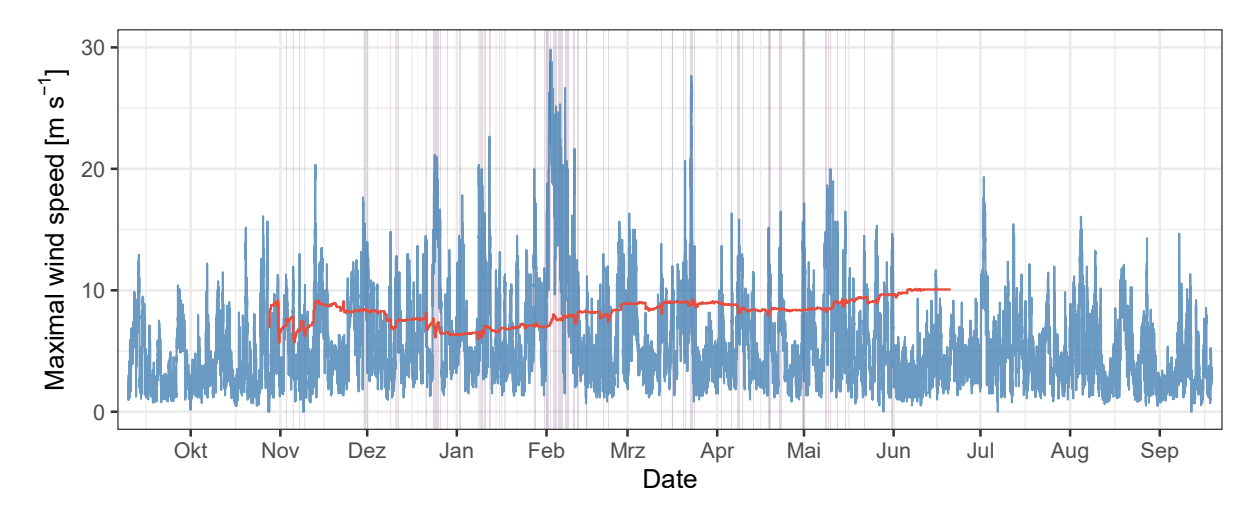


Figure 19: Temporal variability of the dynamic wind speed threshold (red) together with the maximum wind speed (blue) from September 2024 to September 2025. The shaded light purple lines represent the identified snowdrift events.

Furthermore, the other thresholds that I implemented were successful, as I was able to identify meaningful snowdrift events. However, some thresholds have filtered out too many events, for example, the minimum duration of 3 hours for an event. I have implemented this threshold to get important snowdrift events as defined by Sturm et al., but it would have been possible to keep all snowdrift events no matter of duration and then search for the important events later (Sturm et al., 2001). This method is supported by the comparison of the mean snow flux with the duration which is grouped by the event intensity (TST). This comparison proves that the mean snow flux doesn't correlate with the duration which also makes sense, because moreover the short-term wind gusts determine the snow flux instead of the event duration (Figure 6). However, the duration determines the overall TST of the event and therefore also the events intensity considering the relocation of snow mass.

Furthermore, the threshold for rain events was meaningful as I correctly identified periods of rain. Nevertheless, the analysis showed that snowdrift events can take place together with rain events. Especially during early February, there are a lot of small snowdrift events that are interrupted by rain events. This weather phenomena at Bayelva station arises from a rapid warming of the Arctic site which causes warm winter cyclones. These storm events transport warm and wet air into the Arctic which results in high liquid precipitation and rain on snow events (Wickström et al., 2020). This is illustrated in the snowdrift event 34 that takes place exactly between two rain events and is characterized by very high wind speeds and temperature up to 3.3 °C (Figure 15).

4.3 Characterization of snowdrift events

4.3.1 Snow flux

The intensity of snow flux is not uniform during the season but moreover dominated by just a few high-intensity events. Even if my 73 identified events differ from each other, 74 % of the snow transport of the whole season is just dominated by 3 of these events. Thereby just one single event accounts for 50% of TST during the whole season from September 2024 to September 2025 (Figure 20). This indicates that most of the other events have a short duration and a relatively low snow flux, compared to the major events. This is also represented in the events summary, in which half of the events last between 3 and 6.5 hours, so are just driven by short-lived strong gusts of wind (Table 3). This finding is also observed in literature, for example Sturm et al. identified 5-8 major events in a typical winter in arctic Alaska (Sturm et al., 2001). Additionally, that pattern seems to be even more pronounced at Bayelva station. This suggests that the seasonal snow transport at Bayelva is especially driven by a few extreme events that can change the snow-water budget fundamentally.

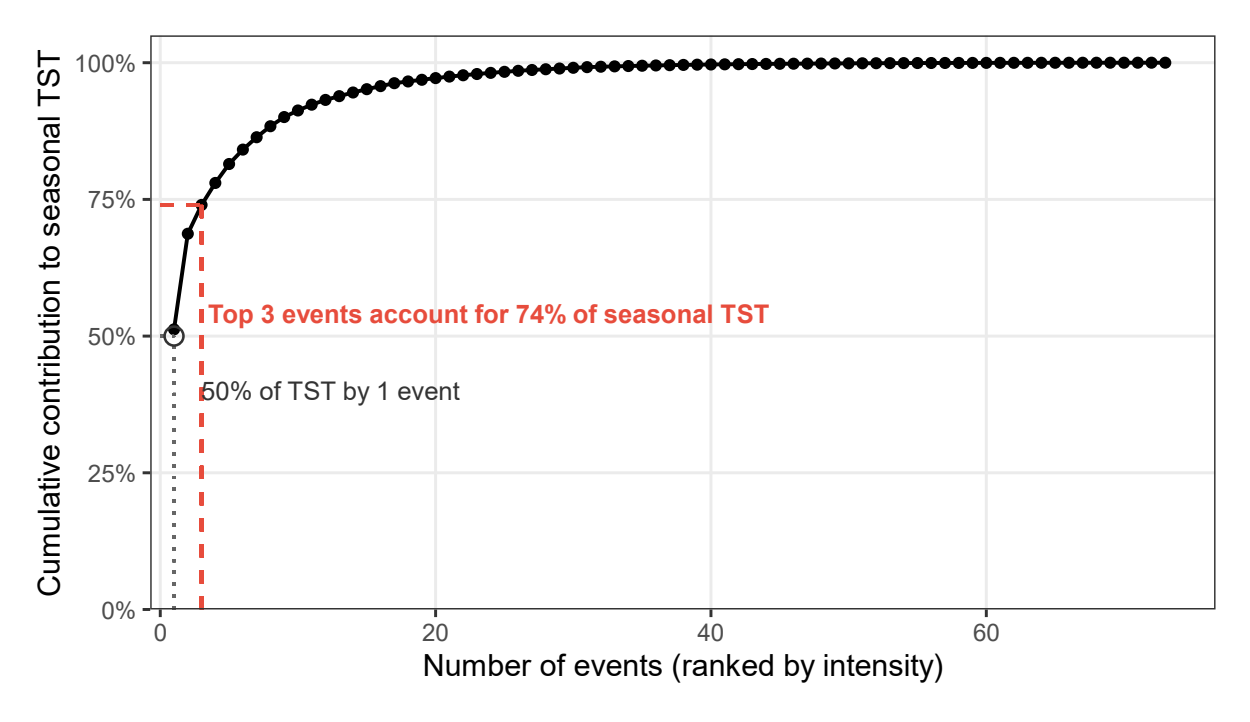


Figure 20: Cumulative contribution of identified snowdrift events ranked by their TST and compared to the total seasonal snow transport during the season from September 2024 to September 2025.

Furthermore, not just the TST over the events is uneven distributed, but also the frequency of events over a timescale (Figure 21). While I identified most snowdrift events in January and February, more TST was transported in March. Also, the event intensity is higher in March, followed by December and February. This temporal distribution of events can result from the seasonal development of the snowpack which has its' lowest density in the end of December to early January (Figure 3). Therefore, the wind speed threshold is

lower and snow can be eroded easier (Figure 19). Also, the solid precipitation is highest in December and February, which explains the high number of events.

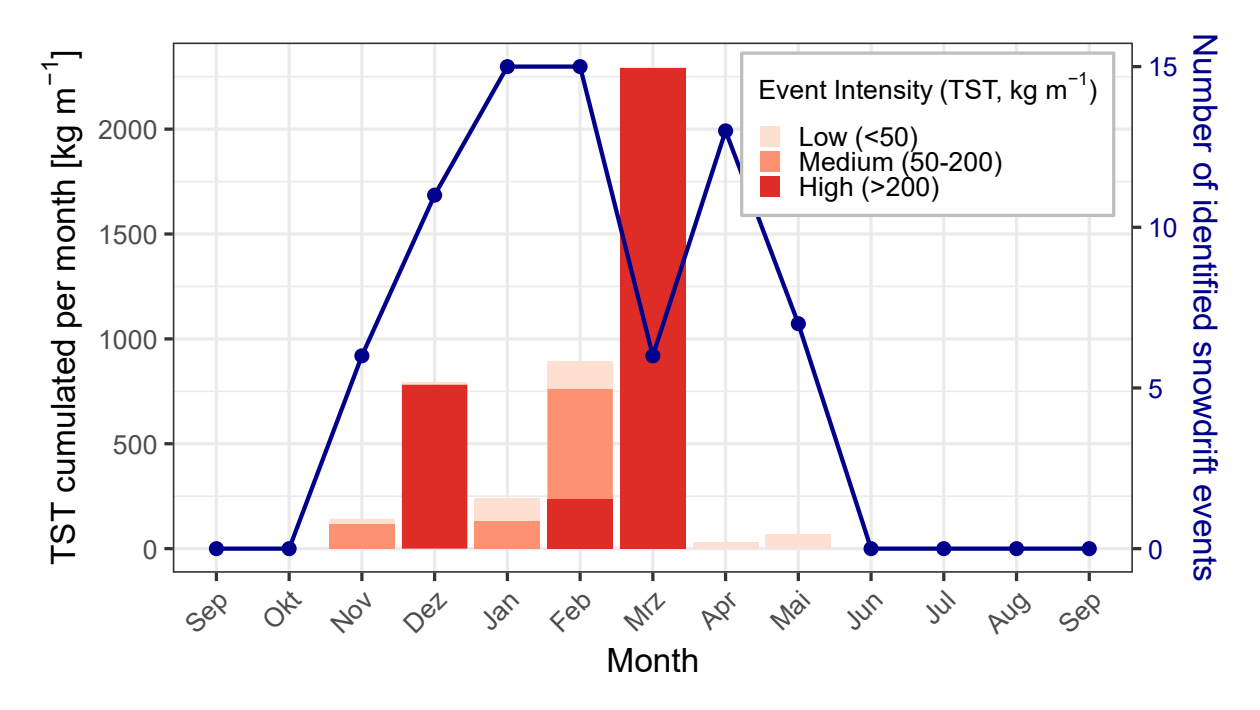


Figure 21: Comparison of monthly snow transport (TST) and the number of identified snowdrift events during the season from September 2024 to September 2025. TST is cumulated per month and represented by stacked bars that are grouped by intensity. Number of identified snowdrift events are represented by blue line.

4.3.2 Wind speed and direction

The results show that the critical wind speed to initialize snowdrift has a great variety. It highly depends on the state of the snowpack which was the limiting factor during non-events (Figure 8). Furthermore, turbulent gusts are responsible for erosion. This is not just present in literature but also confirmed by the model that had a better correlation in frequency with the maximum wind speed (Figure 6) and by the observation that the maximum wind speed is twice as high as the mean wind speed (Table 3) (Pomeroy & Gray, 1995). Nevertheless, even if snowdrift is initiated by short gusts, a long-lasting wind speed is needed to maintain the event.

The direction of the wind determines the spatial patterns of snow transportation, erosion, and deposition. This is influenced by the thin fence that determines the snow depth change for specific stations. The wind might be slower at the BaSnow2019 station which is located leeward behind the corner of the fence, so more snow accumulates. In contrast, the wind at the BaSnow2019 station could be more turbulent behind the fence and then speeds up again towards the station which explains why more snow is eroded. These assumptions could be tested with a detailed wind field measurement at both stations.

4.3.3 Snow characteristics

The limiting factor of snowdrift is the snow density as dense snow is harder to erode even at a high wind speed. Nevertheless, the snow density of the eroded particles is hard to determine as I always calculated the density of the whole snowpack and not just the density from the fresh snow on top that gets eroded. Therefore, the density of the eroded particles is often overestimated and can be faulty calculated also for events with high intensity (Figure 10). During winter period, the density of the snowpack increases naturally, because it is compacted by additional snow, from wind or during elementary processes, for example a compaction due to gravity or by metamorphic processes, e.g. thawing and freezing cycle which increases icing. Some inconsistencies in this increasing snow density in the early accumulation period are caused by the calculation of density and from an alternation of rainy periods and snowy periods (Figure 11).

Furthermore, snow availability is not a limiting factor for snowdrift during the winter months. The rapidly thawing period in June results from the polar day with possibly continuous sunlight and warmer temperatures. Discrepancies between measured solid precipitation but no increasing SWE indicate that sublimation occurred during snowdrift events (Figure 11). This is confirmed by increasing relative humidity during all snowdrift events. Furthermore, the measurements of snow depth are systematically underestimated by around 50% during periods of strong wind due to literature (Athulya et al., 2023).

4.3.4 Air temperature

Air temperature is an additional factor that limits snowdrift, as it affects the binding forces between snow grains. The temperature at Bayelva station is characterized by a moderate winter with outbreaks of both very cold and warm air (Figure 12). The snowdrift intensity is higher at medium temperatures from +1 to -13°C, because lower or higher temperatures increase particle cohesion (Fabricus et al., 2025). With lower temperatures the snow gets icy, whereas higher temperatures lead to melting which both increases density and makes the snow hard to erode.

4.3.5 Precipitation

Solid precipitation is accountable for fresh snow availability and acts as a driver of snowdrift events. Fresh snow has low cohesion and a pronounced crystal structure which increases the surface area. Therefore, a lower wind speed is needed to erode fresh snow (Pomeroy & Gray, 1995). Additionally, the availability of fresh snow influences the intensity of an event. In contrast, liquid precipitation has a more complex effect on the snowpack itself. Rain dramatically increases snow density and cohesion, because the snow will develop an ice crust in cold conditions. This makes the snow very hard to erode even a

long time after a precipitation event. Therefore, no more snowdrift events can occur till fresh snow falls (Figure 3). The remaining probability of snowdrift after a rain event is most likely due to the complex weather conditions that go along with liquid precipitation in winter (Figure 13a). These are big storm systems that can bring liquid as well as solid precipitation together with very high wind speeds (Wickström et al., 2024).

4.4 Single snowdrift events

Overall, the analysis of snowdrift events showed that there is a huge difference between events in their meteorological parameters and snow characteristics as well as their drivers. Even if the averages for the meteorological parameters and snow characteristics during snowdrift events notably differed compared to when no snowdrift event occurred, the events also are very heterogen compared to each other (Figure 7). This great variability suggests that there is no single driver that determines the occurrence of snowdrift and this depends moreover on a complex system of multiple factors, for example the availability of fresh snow, an ideal temperature and sufficient wind speed.

The early and late season events 1 and 73 occurred under snow-limited conditions. The first event took place in the fluctuating phase of rain and snow, so no sufficient snowpack was built yet, therefore the event relied on new snow. In contrast, enough snow was available for the last event, but it was very dense and icy, therefore this also required fresh snow. For both events the wind speed was moderate and would not have been sufficient to erode without new snow.

The major event 52 in March is an example of a wind-driven event, as snowdrift and wind speed followed the same pattern. The high wind speeds over a long time suggest that the event raised from a well-developed wind system that came together with good meteorological conditions. For example, an ideal temperature at around -11 °C and enough available snow. Nevertheless, the snow was very dense with 446 kg m $^{-3}$ during the peak and increased to 490 kg m $^{-3}$ in the end due to a compaction from the high wind speed. As no solid precipitation occurred during the event, it indicates that the loose snow particles were transported in the beginning of the event and came from areas further away during the events' peak. This is also reflected in the snow depth as high erosion as well as sastrugi are visible just in the beginning of the event, whereas no snow depth change is detected in the end. The open landscape at Bayelva station promotes the high snow flux during this event as it provides enough fresh snow and the snowdrift can accelerate with the splash effect that causes a chain reaction (Naaim et al., 1998). Furthermore, it emphasizes that eroded particles can travel in the air over long distances when wind speed stays high.

Event 34 occurs under more complex conditions and shows that snowdrift can occur together between rain events and under warm temperatures. The high wind speed of nearly $30\,\mathrm{m\ s^{-1}}$ together with liquid and solid precipitation is associated with warm winter

cyclones. A huge amount of 3 mm new snowfall provided fresh erodible snow and led to the event.

The consistent rise in relative humidity during all drift events confirms that sublimation occurs. While the absolute amount of moisture added to the air is small due to low temperatures, the relative increase is substantial. This sublimation occurs because lifting snow particles into the air dramatically increases their collective surface area, which is then exposed to unsaturated air which constantly moves due to wind. This process has two important outcomes: it adds moisture to the near-surface atmosphere, potentially contributing to fog, and it results in a mass loss from the snowpack, impacting the local water budget. Nevertheless, the process is self-limiting, as air becomes more saturated, which in turn reduces the rate of further sublimation.

4.5 Validation of Snowdrift Events

The validation results showed that the visual validation was not a suitable method, because of biased analysis and limitations. I confirmed more snowdrift events in the early season from October to January, whereas I could not validate most of the events in the late season from March onward due to light conditions. During polar night, the background of most images was very dark and the camera light illuminated the snow particles against the background, making them easy to see. Unlike during polar day the whole image was very bright which made it hard to see drifting snow particles on the bright snow surface.

Furthermore, the divergent classification according to differing images makes clear that camera 1 is better suitable to detect snowdrift events, as most of them cannot be seen in camera 2. This is because camera 1 looks to the south direction, whereas camera 2 looks to the west. Therefore, the image from camera 2 is often darker during polar night, as the image is dimmed due to the sunset and the contrast is not high enough to see particles.

A better approach is needed to determine snowdrift events independently and more accurately to reduce the bias. This is possible with a scatterometer or a transmissometer which calculates the visibility range using an emitted light beam or light scattering (Chen et al., 2023). The visibility range during snowdrift events should be less than 9.7 kilometers (Savelyev et al., 2006). Nevertheless, this method is more expensive, because additional measurement instruments are needed.

Furthermore, the temporal mismatch between the hourly images from the camera and the 30-minutes averaged peak flux influenced the results dramatically. The maximum snow flux was in 45% of the events between two images. In these cases, I used the first image, so half an hour before the maximum snow flux was measured, because the snowdrift event is initiated at this time. I also checked that all images are still inside the event duration. Nevertheless, the snow flux can be very small so I cannot recognize it

visually. Furthermore, all maximum snow flux values are averaged over the 30-minute period, therefore the resolution of the image doesn't match the timing of the real peak flux. For this reason, a better temporal resolution of the camera is necessary.

4.6 Limitations

Even though the analysis revealed valuable insights, it still is important to account for the limitations of the FC4 device. As I only examine one sensor, the values can't be compared to another sensor and therefore I can't specify the accuracy of the snow flux. Furthermore, there can be potential errors and disturbances that affect the measurements as the FC4 is an acoustic instrument. This can be vibrations from the supporting structure or nearby machines and animals (ISAW, 2020b). Therefore, the sensor can mistaken unrelated vibrations as particle collision. Even if wind speed should be filtered by the sensor, it is possible that in very turbulent periods wind might be counted as snow particles or at least accelerate the measured flux. Particularly the very poor accuracy of the wind speed from the FC4 sensor indicates that wind may have influenced the snow drift measurements. Furthermore, the accuracy of the major snowdrift event in March cannot be determined, because the snow flux exceeded the physical limits. Even if I confirmed the event, the snow flux may have been overestimated.

5 Conclusion

During this thesis, I performed a quality assessment, defined and identified snowdrift events, modeled the erosion flux, analyzed the characteristics of snowdrift events and validated them. A critical result was that the erosion model did not suit my data and was unable to predict the observed erosion. This can have many reasons, because I used a too simplified version and many inaccuracies occurred. For example, I calculated snow density of the whole snowpack which does not reflect the density of the eroded particles. Also, the wind system and its intensity was very simplified in the model. Furthermore, I did not take sublimation into account. Also, the reference data was not comparable to the modeled erosion, as the erosion derived from snow depth change included measurements from sastrugi.

The analysis of my 73 identified snowdrift events showed many differences between the characteristics of the events. I detected multiple drivers and limits of snowdrift events, for example wind speed, snow density, precipitation and temperature. Mainly a complex interplay between meteorological factors and snow parameters led to snowdrift. Even if I just looked at the important events in detail, most of the snowdrift events are small and short-lived. However, my most important finding was that just a few big events account for a huge amount of transported snow throughout the season. This not just changes the landscape, but it has a big impact on the grounds' thermal regime and affects permafrost as well as glaciers. Nevertheless, the validation of snowdrift events was biased by multiple factors that influenced the visibility of snow particles. I overlooked mostly small events in the late season. Therefore, it is important to validate the snow flux data independently, for example with a second measurement device to determine the accuracy.

Further research is needed to examine the impact of snowdrift on the cryosphere and water budget. Also, it is important to validate the snow flux data with a second sensor to determine the accuracy on site. Additionally, it would be interesting to analyze major snow transport routes and examine locations of huge erosion and accumulation more detailed. As my results also highlighted small scale differences in accumulation and erosion, especially together with the fence at study site, it is important to gain a deeper understanding of these micro-scale processes. Furthermore, as I did not quantify sublimation in this thesis, this would be another aspect that changes the snow mass balance and could be considered in future research.

41 Conclusion

6 Literature

Akitaya, E. (1974). Studies on depth hoar. *Contributions from the Institute of Low Temperature Science*, 26, 1-67.

Alduchov, O. A., & Eskridge, R. E. (1996). Improved Magnus form approximation of saturation vapor pressure. Journal of Applied Meteorology (1988-2005), 601-609. https://www.jstor.org/stable/26187406

Amory, C. (2020). Drifting-snow statistics from multiple-year autonomous measurements in Adélie Land, East Antarctica. The Cryosphere, 14(5), 1713-1725. https://doi.org/10.5194/tc-14-1713-2020.

Anderson, R. S., & Haff, P. K. (1991). Wind modification and bed response during saltation of sand in air. In Aeolian Grain Transport 1: Mechanics (pp. 21-51). Vienna: Springer Vienna. https://doi.org/10.1007/978-3-7091-6706-9_2.

Arctic Portal (2025). Where is the Arctic?. Online: https://arcticportal.org/the-arctic-portlet/where-is-the-arctic [last access: 10.10.2025].

Athulya, R., Nuncio, M., Chatterjee, S., Vidya, P. J. (2023). Characteristics of mean and extreme precipitation in Ny Ålesund, Arctic. Atmospheric Research, 295, 106989. https://doi.org/10.1016/j.atmosres.2023.106989.

Baggaley, D. G., Hanesiak, J. M. (2005). An empirical blowing snow forecast technique for the Canadian Arctic and the Prairie Provinces. Weather and forecasting, 20(1), 51-62. https://doi.org/10.1175/WAF-833.1.

Benn, D. I., & Evans, D. J. A. (2010). Glaciers and Glaciation. Hodder Education. London, UK, 802. https://doi.org/10.4324/9780203785010.

Boike, J., Grünberg, I., Miesner, F., Bornemann, N., Cable, W. L. (2025). Meteorological observations at Bayelva Station in 2024 (level 1) [dataset]. PANGAEA, https://doi.org/10.1594/PANGAEA.980876, In: Boike, J., Grünberg, I., Miesner, F., Bornemann, N., Cable, W. L. (2022). Continuous measurements in soil and air at the permafrost long-term observatory at the Bayelva station near Ny-Ålesund (2018 et seq) [dataset bundled publication]. PANGAEA, https://doi.org/10.1594/PANGAEA.948951.

Boike, J., Juszak, I., Lange, S., Chadburn, S., Burke, E., Overduin, P. P., Roth, K., Ippisch, O., Bornemann, N., Stern, L., Gouttevin, I., Hauber, E., Westermann, S. (2018). A 20-year record (1998–2017) of permafrost, active layer and meteorological conditions at a high Arctic permafrost research site (Bayelva, Spitsbergen). Earth System Science Data, 10(1), 355-390. https://doi.org/10.5194/essd-10-355-2018.

Bokhorst, S., Pedersen, S. H., Brucker, L., Anisimov, O., Bjerke, J. W., Brown, R. D., Ehrich, D., Essery, R. L. H., Heilig, A., Ingvander, S., Johansson, C., Johansson, M., Jónsdóttir, I. S., Inga, N., Luojus, K., Macelloni, G., Mariash, H., McLennan, D., Rosqvist, G. N., Sato, A.,

Savela, H., Schneebeli, M., Sokolov, A., Sokratov, S. A., Terzago, S., Vikhamar-Schuler, D., Williamson, S., Qiu, Y. & Callaghan, T. V. (2016). Changing Arctic snow cover: A review of recent developments and assessment of future needs for observations, modelling, and impacts. *Ambio*, 45(5), 516-537. https://doi.org/10.1007/s13280-016-0770-0.

Callaghan, T. V., Johansson, M., Brown, R. D., Groisman, P. Y., Labba, N., Radionov, V., Barry, R. G., Bulygina, O. N., Essery, R. L. H., Frolov, D. M., Golubev, V. N., Grenfell, T. C., Petrushina, M. N., Razuvaev, V. N., Robinson, D. A., Romanov, P., Shindell, D., Shmakin, A. B., Sokratov, S. A., Warren, S. & Yang, D. (2011). The changing face of Arctic snow cover: A synthesis of observed and projected changes. *Ambio*, *40*(Suppl 1), 17-31. https://doi.org/10.1007/s13280-011-0212-y.

Campbell Scientific (2021). CS725 Snow Water Equivalency Sensor. Product Manual. https://s.campbellsci.com/documents/eu/manuals/cs725%20-%20968.pdf [last access: 07.09.2025].

Campbell Scientific (2020). 52203 RM Young Tipping Bucket Raingauge (0.1mm/tip). Product Sheet. https://s.campbellsci.com/documents/eu/product-brochures/b-52203.pdf [last access: 07.09.2025].

Campbell Scientific (2013). SR50 Sonic Ranging Sensor. Instruction Manual. https://www.manualslib.com/download/2423731/Campbell-Sr50.html [last access: 07.09.2025].

Campbell Scientific (2009). Model HMP45C Temperature and Relative Humidity Probe. Instruction Manual. https://s.campbellsci.com/documents/us/manuals/hmp45c.pdf [last access: 07.09.2025].

Chen, L., Shui, Y., Chen, L., Li, M., Chu, J., Shen, X., Zhou, Y & Zhou, J. (2023). Multichannel visibility distribution measurement via optical imaging. In *Photonics* (Vol. 10, No. 8, p. 945). MDPI. https://doi.org/10.3390/photonics10080945.

Chritin, V., Bolognesi, R., Gubler, H. (1999). FlowCapt: a new acoustic sensor to measure snowdrift and wind velocity for avalanche forecasting. Cold Regions Science and Technology, 30(1-3), 125-133. https://doi.org/10.1016/S0165-232X(99)00012-9.

Cierco, F. X., Naaim-Bouvet, F., Bellot, H. (2007). Acoustic sensors for snowdrift measurements: How should they be used for research purposes?. Cold Regions Science and Technology, 49(1), 74-87. https://doi.org/10.1016/j.coldregions.2007.01.002

Cogley, J. G., Arendt, A. A., Bauder, A., Braithwaite, R. J., Hock, R., Jansson, P., Kaser, G., Moller, M., Nicholson, L., Rasmussen, L. A., Zemp, M. (2011). Glossary of glacier mass balance and related terms. (IHP-VII Technical Documents in Hydrology). International Hydrological Programme. https://doi.org/10.5194/tc-7-1287-2013.

Colbeck, S. C. (1986). Classification of seasonal snow cover crystals. *Water Resources Research*, 22(9S), 59-70. https://doi.org/10.1029/WR022i09Sp0059S.

DeepL SE (2025). DeepL Translator [Machine translation software]. https://www.deepl.com/de/translator [last access: 08.09.2025].

Doorschot, J. J. J., Lehning, M., Vrouwe, A. (2004). Field measurements of snow-drift threshold and mass fluxes, and related model simulations. Boundary-Layer Meteorology, 113(3), 347-368. https://doi.org/10.1007/s10546-004-8659-z.

Dormann, C. (2020). Environmental data analysis: an introduction with examples in R. Springer Nature. https://doi.org/10.1007/978-3-030-55020-2.

Dou, T., Xiao, C., Liu, J., Wang, Q., Pan, S., Su, J., Yuan, X., Ding, M., Zhang, F., Xue, K., Bieniek, P. A., Eicken, H. (2021). Trends and spatial variation in rain-on-snow events over the Arctic Ocean during the early melt season. The Cryosphere, 15(2), 883-895. https://doi.org/10.5194/tc-15-883-2021.

Dutra, E., Schär, C., Viterbo, P., Miranda, P. M. (2011). Land-atmosphere coupling associated with snow cover. Geophysical Research Letters, 38(15). https://doi.org/10.1029/2011GL048435.

Essery, R., Morin, S., Lejeune, Y., & Ménard, C. B. (2013). A comparison of 1701 snow models using observations from an alpine site. *Advances in water resources*, *55*, 131-148. https://doi.org/10.1016/j.advwatres.2012.07.013.

Etzelmüller, B. (2013). Recent advances in mountain permafrost research. Permafrost and periglacial Processes, 24(2), 99-107. https://doi.org/10.1002/ppp.1772.

Fabricus, A., Ohara, N., & Ahlenius, K. (2025). Stochastic modeling of blowing snow: Analyzing risk and deposition time dynamics. Cold Regions Science and Technology, 104446. https://doi.org/10.1016/j.coldregions.2025.104446.

Federov, V. P., Zhuravel, V. P., Grinyaev, S. N., & Medvedev, D. A. (2019). Scientific approaches to defining the territorial boundaries of the Arctic. In *IOP conference series: Earth and environmental science* (Vol. 302, No. 1, p. 012012). IOP Publishing. https://doi.org/10.1088/1755-1315/302/1/012012.

Ferrari, C. P., Gauchard, P. A., Aspmo, K., Dommergue, A., Magand, O., Bahlmann, E., ... & Boutron, C. F. (2005). Snow-to-air exchanges of mercury in an Arctic seasonal snow pack in Ny-Ålesund, Svalbard. *Atmospheric Environment*, 39(39), 7633-7645. https://doi.org/10.1016/j.atmosenv.2005.06.058

Filhol, S., & Sturm, M. (2015). Snow bedforms: A review, new data, and a formation model. *Journal of Geophysical Research: Earth Surface*, *120*(9), 1645-1669. https://doi.org/10.1002/2015JF003529

Gisnås, K., Westermann, S., Schuler, T. V., Litherland, T., Isaksen, K., Boike, J., Etzelmüller, B. (2014). A statistical approach to represent small-scale variability of permafrost temperatures due to snow cover. The Cryosphere, 8(6), 2063-2074. https://doi.org/10.5194/tc-8-2063-2014.

Goodrich, L. E. (1982). The influence of snow cover on the ground thermal regime. Canadian geotechnical journal, 19(4), 421-432. https://doi.org/10.1139/t82-047.

Google (2025). Gemini 2.5 Pro [Large language model]. Retrieved from https://aistudio.google.com [last access: 10.10.2025].

Goosse, H., Kay, J. E., Armour, K. C., Bodas-Salcedo, A., Chepfer, H., Docquier, D., Jonko, A., Kushner, P. J., Lecomte, O., Massonnet, F., Park, H-S., Pithan, F., Svensson, G., Vancoppenolle, M. (2018). Quantifying climate feedbacks in polar regions. Nature communications, 9(1), 1919. https://doi.org/10.1038/s41467-018-04173-0.

Gordon, M., Savelyev, S., & Taylor, P. A. (2009). Measurements of blowing snow, part II: Mass and number density profiles and saltation height at Franklin Bay, NWT, Canada. Cold Regions Science and Technology, 55(1), 75-85. https://doi.org/10.1016/j.coldregions.2008.07.001.

Gruber, S., King, L., Kohl, T., Herz, T., Haeberli, W., Hoelzle, M. (2004). Interpretation of geothermal profiles perturbed by topography: The Alpine permafrost boreholes at Stockhorn Plateau, Switzerland. Permafrost and Periglacial Processes, 15(4), 349-357. https://doi.org/10.1002/ppp.503.

Grünberg, I., Groenke, B., Westermann, S., & Boike, J. (2024). Permafrost and active layer temperature and freeze/thaw timing reflect climatic trends at Bayelva, Svalbard. Journal of Geophysical Research: Earth Surface, 129(7), e2024JF007648. https://doi.org/10.1029/2024JF007648.

Haapala, J., Lensu, M., Dumont, M., Renner, A. H., Granskog, M. A., & Gerland, S. (2013). Small-scale horizontal variability of snow, sea-ice thickness and freeboard in the first-year ice region north of Svalbard. *Annals of Glaciology*, *54*(62), 261-266. https://doi.org/10.3189/2013AoG62A157

Haeberli, W. (1973). Die Basis-Temperatur der winterlichen Schneedecke als moglicher Indikator fur die Verbreitung von Permafrost in den Alpen. Zeitschrift fur Gletscherkunde und Glazialgeologie, 9, 221-227.

Harris, C., Arenson, L. U., Christiansen, H. H., Etzelmüller, B., Frauenfelder, R., Gruber, S., Haeberli, W., Hauck, C., Höl zle, M., Humlum, O., Isaksen, K., Kääb, A., Lehning, M., Lütschg, M. A., Matsuoka, N., Murton, J., Nötzli, J., Phillips, M., Ross, N., Seppälä, M., Springman, S., and Vonder Muhll, D. (2009). Permafrost and climate in Europe: Monitoring and modelling thermal, geomorphological and geotechnical responses. Earth-Science Reviews, 92(3-4), 117-171. https://doi.org/10.1016/j.earscirev.2008.12.002.

Hodson, T. O. (2022). Root mean square error (RMSE) or mean absolute error (MAE): When to use them or not. *Geoscientific Model Development Discussions*, 2022, 1-10. https://doi.org/10.5194/gmd-15-5481-2022.

Isaksen, K., Ødegård, R. S., Etzelmüller, B., Hilbich, C., Hauck, C., Farbrot, H., Eiken, T., Hygen, H. O., Hipp, T. F. (2011). Degrading mountain permafrost in southern Norway: spatial and temporal variability of mean ground temperatures, 1999–2009. Permafrost and Periglacial Processes, 22(4), 361-377. https://doi.org/10.1002/ppp.728.

ISAW (2020a). ISAW CAM user guide V2.14. https://www.isaw-products.com/wp-content/uploads/2020/07/21-ISAW_User_Guide_V2.14.pdf, [last access: 15.07.2025].

ISAW (2020b). FlowCapt FC4 short product description V4.0. https://www.isaw-products.com/wp-content/uploads/2020/12/01-FlowCapt_FC4_Short_Product_Description_V4.0.pdf, [last access: 15.07.2025].

ISAW (2005). FlowCapt. Remote automatic snow & weather monitoring. Technical specifications. http://dev.isaw.ch/pdf/en/flowcapt.pdf, [last access: 15.07.2025].

Ishikawa, M. (2003). Thermal regimes at the snow–ground interface and their implications for permafrost investigation. Geomorphology, 52(1-2), 105-120. https://doi.org/10.1016/S0169-555X(02)00251-9.

Jaedicke, C., & Gauer, P. (2005). The influence of drifting snow on the location of glaciers on western Spitsbergen, Svalbard. *Annals of Glaciology*, 42, 237-242. https://doi.org/10.3189/172756405781812628.

Jaedicke, C. (2001). Acoustic snowdrift measurements: experiences from the FlowCapt instrument. Cold Regions Science and Technology, 32(1), 71-81. https://doi.org/10.1016/S0165-232X(01)00017-9.

Jennings, K. S., Winchell, T. S., Livneh, B., Molotch, N. P. (2018). Spatial variation of the rain–snow temperature threshold across the Northern Hemisphere. Nature communications, 9(1), 1148. https://doi.org/10.1038/s41467-018-03629-7.

Jentzsch, K., Bornemann, N., Cable, W., Gallet, J. C., Lange, S., Westermann, S. and Boike, J. (2020). Near real-time observations of snow water equivalent for SIOS on Svalbard – (SWESOS). https://doi.org/10.5281/zenodo.4146835.

Lambrecht meteo GmbH (2025). Rain[e]H3 Wiegender Niederschlagssensor. Product-View. https://www.lambrecht.net/scripts/pdf.php?id=50&lang=german [last access: 07.09.2025].

López-Moreno, J. I., Boike, J., Sanchez-Lorenzo, A., Pomeroy, J. W. (2016). Impact of climate warming on snow processes in Ny-Ålesund, a polar maritime site at Svalbard. Global and Planetary Change, 146, 10-21. https://doi.org/10.1016/j.gloplacha.2016.09.006.

Luetschg, M., Stoeckli, V., Lehning, M., Haeberli, W., Ammann, W. (2004). Temperatures in two boreholes at Flüela Pass, Eastern Swiss Alps: the effect of snow redistribution on permafrost distribution patterns in high mountain areas. Permafrost and Periglacial Processes, 15(3), 283-297. https://doi.org/10.1002/ppp.500.

Luetschg, M., Lehning, M., Haeberli, W. (2008). A sensitivity study of factors influencing warm/thin permafrost in the Swiss Alps. Journal of Glaciology, 54(187), 696-704. https://doi.org/10.3189/002214308786570881.

Maturilli, Marion (2020). Continuous meteorological observations at station Ny-Ålesund (2011-08 et seq) [dataset publication series]. Alfred Wegener Institute - Research Unit Potsdam, PANGAEA, https://doi.org/10.1594/PANGAEA.914979, [data retrieved on 30.06.2025].

Mäkiranta, E., Vihma, T., Sjöblom, A., & Tastula, E. M. (2011). Observations and modelling of the atmospheric boundary layer over sea-ice in a Svalbard Fjord. *Boundary-Layer Meteorology*, *140*(1), 105-123. https://doi.org/10.1007/s10546-011-9609-1.

McGuire, A. D., Lawrence, D. M., Koven, C., Clein, J. S., Burke, E., Chen, G., Jafarovh, E., MacDougall, A. H., Marchenko, S., Nicolsky, D., Peng, S., Rinke, A., Ciaisk, P., Gouttevin, I., Hayes, D. J., Ji, D., Krinner, G., Moore, J. C., Romanovskyi, V., Schädel, C., Schaeferv, K., Schuur, E. A. G., Zhuang, Q. (2018). Dependence of the evolution of carbon dynamics in the northern permafrost region on the trajectory of climate change. Proceedings of the National Academy of Sciences, 115(15), 3882-3887. https://doi.org/10.1073/pnas.1719903115.

Meredith, M., M. Sommerkorn, S. Cassotta, C. Derksen, A. Ekaykin, A. Hollowed, G. Kofinas, A. Mackintosh, J. Melbourne-Thomas, M.M.C. Muelbert, G. Ottersen, H. Pritchard, and E.A.G. Schuur, 2019: Polar Regions. In: IPCC Special Report on the Ocean and Cryosphere in a Changing Climate [H.-O. Pörtner, D.C. Roberts, V. Masson-Delmotte, P. Zhai, M. Tignor, E. Poloczanska, K. Mintenbeck, A. Alegría, M. Nicolai, A. Okem, J. Petzold, B. Rama, N.M. Weyer (eds.)]. Cambridge University Press, Cambridge, UK and New York, NY, USA, pp. 203–320. https://doi.org/10.1017/9781009157964.005.

Naaim, M., Naaim-Bouvet, F., & Martinez, H. (1998). Numerical simulation of drifting snow: erosion and deposition models. *Annals of glaciology*, *26*, 191-196. https://doi.org/10.3189/1998AoG26-1-191-196.

Norwegian Polar Institute (2025). *TopoSvalbard web map*. Online: https://toposvalbard.npolar.no/?lat=78.92094&long=11.83327&zoom=12&layer=map [last access: 01.10.2025].

Notz, D., Stroeve, J. (2016). Observed Arctic sea-ice loss directly follows anthropogenic CO2 emission. Science, 354(6313), 747-750. https://doi.org/10.1126/science.aag2345.

Ovesen, M. J. S. (2024). Snowdrift Analysis using FlowCapt FC4 and LiDAR Data at Fv. 53 Tyin-Årdal. *Master's thesis, UiT (The Arctic university of Norway)*. https://hdl.handle.net/10037/33805

Pomeroy, J. W., Marsh, P., Gray, D. M. (1997). Application of a distributed blowing snow model to the Arctic. Hydrological processes, 11(11), 1451-1464.

https://doi.org/10.1002/(SICI)1099-1085(199709)11:11%3C1451::AID-HYP449%3E3.0.C O;2-Q, [last access: 15.07.2025].

Pomeroy, J., & Gray, D. M. (1995). Snowcover: Accumulation, relocation, and management. National Hydrology Research Institute. https://hdl.handle.net/10388/15161, [last access: 16.07.2025].

Pithan, F., Mauritsen, T. (2014). Arctic amplification dominated by temperature feedbacks in contemporary climate models. Nature geoscience, 7(3), 181-184. https://doi.org/10.1038/ngeo2071.

R. M. Young Company (2000). Wind Monitor-HD Alpine MODEL 05108-45. Instructions. https://www.youngusa.com/wp-content/uploads/2013/05/05108-45-90E.pdf [last access: 07.09.2025].

Radić, V., Bliss, A., Beedlow, A. C., Hock, R., Miles, E., & Cogley, J. G. (2013). Regional and global projections of twenty-first century glacier mass changes in response to climate scenarios from global climate models. Climate Dynamics, 42(1), 37-58. https://doi.org/10.1007/s00382-013-1719-7.

Razali, N. M., Wah, Y. B. (2011). Power comparisons of shapiro-wilk, kolmogorov-smirnov, lilliefors and anderson-darling tests. Journal of statistical modeling and analytics, 2(1), 21-33.

https://www.nbi.dk/~petersen/Teaching/Stat2017/Power_Comparisons_of_Shapiro-Wilk_Kolmogorov-Smirn.pdf, [last access: 17.07.2025].

Richter-Menge, J., Overland, J. E., Mathis, J. T., Osborne, E. B. (2017). Arctic Report Card 2017: Arctic shows no sign of returning to reliably frozen region of recent past decades. [Available at: www.arctic.noaa.gov/Report-Card].

Saigger, M., Sauter, T., Schmid, C., Collier, E., Goger, B., Kaser, G., Prinz, R., Voordendag, A., Mölg, T. (2024). A drifting and blowing snow scheme in the weather research and forecasting model. Journal of Advances in Modeling Earth Systems, 16(6), e2023MS004007. https://doi.org/10.1029/2023MS004007.

Sauter, T., Möller, M., Finkelnburg, R., Grabiec, M., Scherer, D., Schneider, C. (2013): Snowdrift modelling for the Vestfonna ice cap, north-eastern Svalbard. The Cryosphere, 7(4), 1287-1301. https://doi.org/10.5194/tc-7-1287-2013.

Savelyev, S. A., Gordon, M., Hanesiak, J., Papakyriakou, T., & Taylor, P. A. (2006). Blowing snow studies in the Canadian Arctic shelf exchange study, 2003–04. *Hydrological Processes: An International Journal*, 20(4), 817-827. https://doi.org/10.1002/hyp.6118.

Serreze, M. C., Barry, R. G. (2011). Processes and impacts of Arctic amplification: A research synthesis. Global and planetary change, 77(1-2), 85-96. https://doi.org/10.1016/j.gloplacha.2011.03.004.

Setra Systems, Inc. (2019). Model 278 Barometric Pressure Transducer. Product Sheet. https://www.setra.com/hubfs/Product_Data_Sheets/Setra_Model_278_Data_Sheet.pdf [last access: 07.09.2025].

Stuecker, M. F., Bitz, C. M., Armour, K. C., Proistosescu, C., Kang, S. M., Xie, S. P., Kim, D., McGregor, S., Zhang, W., Zhao, S., Cai, W., Dong, Y., Jin, F. F. (2018). Polar amplification dominated by local forcing and feedbacks. Nature Climate Change, 8(12), 1076-1081. https://doi.org/10.1038/s41558-018-0339-y.

Stull, R. B. (1988). An introduction to boundary layer meteorology (Vol. 13). Springer Science & Business Media, 671. https://dx.doi.org/10.1007/978-94-009-3027-8.

Sturm, M., Taras, B., Liston, G. E., Derksen, C., Jonas, T., & Lea, J. (2010). Estimating snow water equivalent using snow depth data and climate classes. Journal of Hydrometeorology, 11(6), 1380-1394. https://doi.org/10.1175/2010JHM1202.1.

Sturm, M., Liston, G. E., Benson, C. S., & Holmgren, J. (2001). Characteristics and growth of a snowdrift in Arctic Alaska, USA. Arctic, Antarctic, and Alpine Research, 33(3), 319-329. https://doi.org/10.1080/15230430.2001.12003436.

Trouvilliez, A., Naaim-Bouvet, F., Bellot, H., Genthon, C., Gallée, H. (2015). Evaluation of the FlowCapt acoustic sensor for the aeolian transport of snow. Journal of Atmospheric and Oceanic Technology, 32(9), 1630-1641. https://doi.org/10.1175/JTECH-D-14-00104.1.

Trouvilliez, A., Naaim-Bouvet, F., Genthon, C., Piard, L., Favier, V., Bellot, H., Agosta, C., Palerme, C., Amory, C., Gallée, H. (2014). A novel experimental study of aeolian snow transport in Adelie Land (Antarctica). Cold regions science and technology, 108, 125-138. https://doi.org/10.1016/j.coldregions.2014.09.005.

Upton, G. J. G., & Rahimi, A. R. (2003). On-line detection of errors in tipping-bucket raingauges. *Journal of Hydrology*, 278(1-4), 197-212. https://doi.org/10.1016/S0022-1694(03)00142-2

van Pelt, W., Pohjola, V., Pettersson, R., Marchenko, S., Kohler, J., Luks, B., Hagen, J. O., Schuler, T. V., Dunse, T., Noël, B., Reijmer, C. (2019). A long-term dataset of climatic mass balance, snow conditions, and runoff in Svalbard (1957–2018). *The Cryosphere*, *13*(9), 2259-2280. https://doi.org/10.5194/tc-13-2259-2019.

von Kármán, T. (1930). Mechanische Anlichkeit und Turbulenz. *Nachrichten von der Gesellschaft der Wissenschaften zu Göttingen, Mathematisch-Physikalische Klasse*, 1930, 58-76. https://eudml.org/doc/59299.

Voordendag, A., Goger, B., Prinz, R., Sauter, T., Mölg, T., Saigger, M., Kaser, G. (2024). A novel framework to investigate wind-driven snow redistribution over an Alpine glacier: combination of high-resolution terrestrial laser scans and large-eddy simulations. The Cryosphere, 18(2), 849-868. https://doi.org/10.5194/tc-18-849-2024.

Walter, M. T., McCool, D. K., King, L. G., Molnau, M., & Campbell, G. S. (2004). Simple snowdrift model for distributed hydrological modeling. Journal of Hydrologic Engineering, 9(4), 280-287. https://doi.org/10.1061/(ASCE)1084-0699(2004)9:4(280).

Yang, S., Zhang, M., Pei, W., Melnikov, A., Zhang, Z., & You, Z. (2022). Numerical study on snow erosion and deposition around an embankment with a snow fence under snowfall conditions. *Aeolian Research*, 56, 100798. https://doi.org/10.1016/j.aeolia.2022.100798.

Zhang, T., Barry, R. G., Haeberli, W. (2001). Numerical simulations of the influence of the seasonal snow cover on the occurrence of permafrost at high latitudes. Norsk Geografisk Tidsskrift-Norwegian Journal of Geography, 55(4), 261-266. https://doi.org/10.1080/00291950152746621.

Zhang, W., He, J., Chen, A. A., Wu, X., Shen, Y. (2022). Observations of drifting snow using flowcapt Sensors in the southern altai mountains, Central Asia. Water, 14(6), 845. https://doi.org/10.3390/w14060845.

7 Appendix

7.1 Dataset overview

Table 5: Overview of the used datasets, sensors and parameters with accuracy.

Dataset and Temporal Resolution	Parameter	Device Manu- facturer, Type	Accuracy	Additional Information
BaMet2019 data averaged over 30-minute period,	Wind Speed [m/s]	Young, 05108-45	Standard Accuracy: ± 0.3 m/s	Range: 0 – 100 m/s (R.M. Young Company, 2000)
precipitation data summed over 30- minute period	Temperature in 2m height [°C]	Vaisala, HMP45C	±0.3 °C for 0°C, ±0.4 °C for -20°C, ±0.2 °C for 20 °C	Range: -40 to +60 °C (Campbell Scientific, 2009)
	Relative Humidity in 2m height [%]	Vaisala, HMP45C	at 20°C: ±2% from 0-90% RH, ±3% from 90- 100% RH	Temperature Dependence of RH: ±0.05/°C (Campbell Scientific, 2009)
	Liquid Precipitation (tipping bucket) [mm]	Young, Raingaug e 52203	±2% up to 25mm/h, ±3% up to 50 mm/h	(Campbell Scientific, 2020)
	Liquid and Solid Precipitation (WP)	Lambrec ht, rain[e]H3	±1% for rain < 6 mm/min und ±2% for rain ≥ 6 mm/min; maximal resolution: 0.001 mm	(Lambrecht meteo GmbH, 2025)
	Snow Depth [m]	Campbel l, SR50	±1 cm or 0.4% of distance to target (whichever is greater)	_
	Pressure [hPa]	Setra, 278	±1.5hPa for 800- 1100 hPa and -40 to +60 °C	Range: 500 – 1100 hPa (Setra Systems, Inc. (2019)
BaSnow2019 data averaged over 6- hour period	Snow Depth [m]	Campbel l, SR50	±1 cm or 0.4% of distance to target (whichever is greater)	Range: 0.5-10m (Campbell Scientific, 2013)

51 Appendix

Dataset and Temporal Resolution	Parameter	Device Manu- facturer, Type	Accuracy	Additional Information
	Snow water equivalent [mm]	Campbel I, CS725	±15mm for 0 to 300 mm, ±15% for 300 to 600 mm	Range: 0- 600mm of water equivalency (Campbell Scientific, 2021)
BaSnow2024 data averaged over 30- minute period	Snow Flux [g m ⁻² s ⁻¹]	ISAW, FlowCapt FC4	±5% variability between sensors; maximal resolution: 0.001 g m ⁻² s ⁻¹	Range: 0-250 g m ⁻² s ⁻¹ (ISAW, 2020b)

7.2 Use of Al

I used the AI language model Google Gemini (Google, 2024) for my data analysis as well as for the creation of figures in R. In only used AI as a supportive tool and critically reviewed and validated the output before I implemented this in my code. I used the assistance of AI for the following processes:

- Code writing in R. This includes the correction of errors in my R code, new code development, the creation of figures, structuring of my code as well as feedback and improvement of my existing code.
- Giving feedback to my written text, help for structuring my paragraphs and implementing feedback from others.

Additionally, I used the translation AI DeepL (DeepL SE, 2024) to assist in translating single sentences and a few paragraphs of my written draft text from German to English and improve linguistic correctness.

The structure of this thesis, as well as the conceptual design of my methods and the interpretation of the results is my work and were not done with AI. I used the assistance of AI just for the above-mentioned aspects.

53 Appendix

7.3 Declaration of originality

I hereby declare that I have not submitted this thesis or parts thereof for any other examination or academic credit, and that I have written it independently, using only the specified literature and resources.

I affirm that all passages quoted verbatim from other works, as well as those closely paraphrasing the ideas of other authors, have been clearly marked and the corresponding sources have been cited. All internet sources, graphics, tables, and images that have been reproduced either unchanged or in a modified form have been duly acknowledged as such.

Furthermore, I affirm that I have documented the use of AI in this work in accordance with the current regulations of the examination board.

I am aware that any breach of these principles will be treated as an act of academic misconduct or an attempt at deception.

Ich erkläre, dass ich die vorliegende Arbeit oder Teile davon nicht für andere Prüfungsund Studienleistungen eingereicht, selbständig und nur unter Verwendung der angegebenen Literatur und Hilfsmittel angefertigt habe.

Ich versichere, dass ich alle von anderen Autorinnen und Autoren wörtlich übernommenen Stellen wie auch die sich an die Gedankengänge anderer Autorinnen und Autoren eng anlehnenden Ausführungen der vorliegenden Arbeit besonders gekennzeichnet und die entsprechenden Quellen angegeben habe.

Sämtliche Internetquellen, Grafiken, Tabellen und Bilder, die ich unverändert oder abgewandelt wiedergegeben habe, habe ich als solche kenntlich gemacht.

Zusätzlich versichere ich, dass ich den Prozess und das Ergebnis eines KI-Einsatzes gemäß der Ausführungsbestimmung des Prüfungsausschusses in der seiner jeweils geltenden Form dokumentiert habe. Bei der Erstellung dieser Arbeit habe ich durchgehend eigenständig gearbeitet.

Mir ist bekannt, dass Verstöße gegen diese Grundsätze als Täuschungsversuch bzw. Täuschung geahndet werden.

2025/10/16

Date/ Datum

Signature/ Unterschrift